STRUCTURAL RESPONSE OF AN UNDERGROUND DOUBLE-SHELL TANK TO A HYDROGEN BURN EVENT

Edward A. Rodriguez

Nuclear Systems Design & Analysis Group
Technology & Safety Assessment Division
Los Alamos National Laboratory

Thomas A. Butler
Wilbur D. Birchler

Engineering Analysis Group
Engineering Sciences & Applications Division
Los Alamos National Laboratory

March 1995

LOS ALAMOS NATIONAL LABORATORY

LA-UR-95-941

STRUCTURAL RESPONSE OF AN UNDERGROUND DOUBLE-SHELL TANK TO A HYDROGEN BURN EVENT

by

E. A. Rodriguez, T. A. Butler, and W. D. Birchler

EXECUTIVE SUMMARY

For the past 5 decades, high-level radioactive wastes generated from defense-related operations have been stored in underground tanks at the Hanford Site in Richland, Washington. Over the years, several of these tanks have been observed to generate and expel concentrations of hydrogen, ammonia, nitrous oxide, and nitrogen that are within the flammability limit. The potentially hazardous mixture of gas and solids generation is a result of radiolytic decay and thermal chemical reaction. A potential spark ignition source causing a deflagration leads to concerns about the structural integrity. Furthermore, the potential for gas release events (GREs) with a burn to occur greatly increases with increasing activities in tank maintenance and gas mitigation operations. This study focuses on the dynamic structural response of high-level waste Tank 241-SY-101 subjected to a GRE with a burn.

Analyses with the Hydrogen Mixing Study/Transient Reactor Analysis Code have shown that the rate of pressurization during a burn event is very sensitive to the spark ignition source location in the double-shell tank. Dynamic structural analyses have shown that burn pressure transients, initiated with a spark ignition source located at the waste surface, attain gradual pressurization rates for a given gas release volume. With current assumptions of possible spark ignition source location in the dome space, higher rates of pressurization have been calculated, leading to a dynamic response that is significantly different than previous results have shown.

During the initial pressure-rise portion of the burn transient, the steel-reinforced concrete dome exhibits comparatively larger deformations than the rest of the tank structure. Furthermore, simple shock response spectra analyses show that dynamic amplification of the dome structure is possible only during a state of material degradation. That is, the purely linear-elastic structure has natural frequencies that are above those where amplification would occur. However, extensive concrete cracking and reinforcing bar yielding is predicted during the pressure transient. This softening tends to increase flexibility and decrease natural frequencies. As such, the structure exhibits amplification because of material degradation.

This document provides details and summary results of structural analyses performed for Tank 101-SY under postulated hydrogen burn conditions. The work is subdivided into three parts, each of which provides analysis results of the structural response under a given hydrogen burn. Summaries of numerical

computations that predict the response of the underground double-shell tank to the burn scenarios are presented, each having different spark ignition source locations. Dynamic response parameters that clearly display the effects of the differing rates of pressurization then are parameterized.

LA-UR-95-941

STRUCTURAL RESPONSE OF AN UNDERGROUND DOUBLE-SHELL TANK TO A HYDROGEN BURN EVENT

by

E. A. Rodriguez, T. A. Butler, and W. D. Birchler

ABSTRACT

For the past 5 decades, high-level radioactive wastes generated from defense-related operations have been stored in underground tanks at the Hanford Site in Richland, Washington. Over the years, several of these high-level-waste tanks have been observed to generate and expel concentrations of hydrogen, ammonia, nitrous oxide, and nitrogen that are within the flammability limit. The potentially hazardous mixture of gas and solids generation is a result of radiolytic decay and thermal chemical reaction. As such, the potential for a spark ignition source causing a deflagration leads to concerns about the structural integrity of the tank.

Dynamic structural analyses presented herein show that burn pressure transients, initiated with a spark ignition source located at the waste surface, attain gradual pressurization rates for a given gas release volume. With current assumptions of possible spark ignition source location in the dome space, higher rates of pressurization have been calculated, leading to a structurally dynamic response that significantly is different than previous results have shown.

This paper summarizes numerical computations that predict the response of an underground double-shell tank to burn scenarios, each having different spark ignition source locations. Dynamic response parameters then are parameterized that clearly display the effects of the differing rates of pressurization.

1.0. INTRODUCTION

The structural response of the underground tank to a hydrogen burn is determined by temporal changes in several key parameters, which include the concrete side wall uplift, the vertical displacement of the tank dome, radial displacement of the primary tank side wall, uplift of the primary tank bottom corner, and strains throughout the primary and secondary steel tank liners (see Fig. 1). Although all of
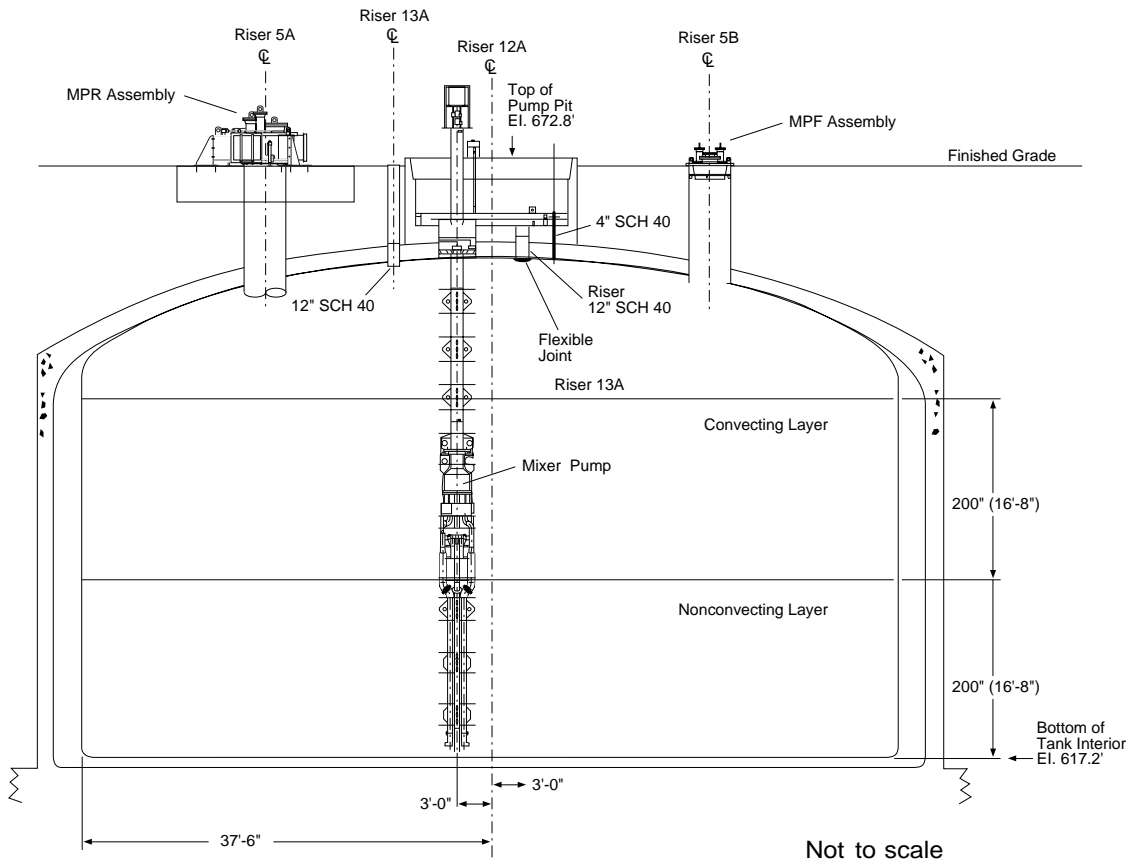
Fig. 1. Cross-sectional view of Tank 101-SY and hydrogen mixer pump.

these parameters are important, the most significant factors are whether the tank maintains its structural integrity below the liquid waste level and whether it maintains overall structural integrity.[1,2]

Numerous pressure-time (P-T) histories have been investigated for gas burns with spark sources located at the waste surface.[2] The original results of these analyses lead us to conclude that the tank can survive the 1.25 times the maximum expected burp (MEB) gas release event (GRE) for the postulated conditions of a surface burn with certain assumptions on gas composition (the MEB corresponds to a 10,480-ft^3 gas release). Originally, the maximum allowable burp (MAB) was defined as 1.25 x MEB. However, changes in gas composition, as well as assumptions of potential spark sources located in the vent systems directly below the dome, have modified the burn P-T history, showing a much steeper pressure-rise time than previously suspected and analyzed. The results of these changes on the structural response of the tank have resulted in a reduction of the MAB.

The spark ignition source located directly below the dome leads to a burn that results in a higher pressurization rate (dP/dt), unlike the original 1.25*MEB case in which the burn front traveled from the waste surface to the dome in a gradual time span.[3]

This document describes both the original baseline reference case and the revised MAB cases. Thus, Tank 101-SY currently is qualified structurally for three separate GREs with a burn corresponding to different gas compositions and different vent-flow areas through the multiport riser (MPR): (1) a 9300-ft^3 GRE based on a conservative gas composition causing a peak burn pressure of 3.92 bar (56.8 psia), with 100% vent-flow area through the MPR; (2) a 8654-ft^3 GRE based on 0% vent-flow area; and (3) a best-estimate gas composition and gas release rate MEB of 10,480 ft^3, which is based on 100 and 0% vent-flow area through the MPR.

The structural analyses contained in this report have been performed with P-T histories from gas burn analyses conducted with the Hydrogen Mixing Study/Transient Reactor Analysis Code (HMS/TRAC) (Ref. 1, App. B). These burn analyses have been performed for given conditions of vent-flow openings through the dome's 42-in. risers. A majority of the analyses assumed a vent-flow area of a fully open 42-in. riser, or 100% area. HMS/TRAC P-T history transients have been developed and compared for both a fully open 42-in. riser and for the MPR with 100% flow-through area. Both of these cases result in identical pressurization rates, peak pressures, and an overall trend of the P-T history transient. Therefore, any reference made herein to a fully open 42-in. riser is synonymous with a 100% vent-flow area through the MPR. The differential between 0 and 100% venting is not significant when converted to gas volume or waste level.

With the installation of the MPR, vent-flow areas can be <100% of a 42-in. riser opening because the MPR can be fully loaded with tank-monitoring equipment. If the MPR has a full complement of tank-monitoring equipment installed, the MPR vent-flow area is reduced to 66% of the total. Furthermore, confirmatory-type analyses were performed to assess the efficiency of installing two MPRs, thus potentially allowing a 200% vent-flow area. This was done to substantiate whether the MAB gas volume could be raised above that of the MEB. For a given gas release volume with different vent-flow areas, the pressurization rate (dP/dt) remains unchanged. However, the peak pressure increases slightly with decreasing vent-flow areas. Therefore, the 200% vent-flow area analysis was performed to evaluate whether the peak pressure would be reduced substantially such that a higher GRE volume could be maintained. The results of the confirmatory-type analyses concluded that the tank pressurization was quite insensitive to vent-flow areas. The conclusion is that no benefit would be derived from adding another MPR in an effort to increase the MAB above the MEB volume.

This document presents the results of the structural analyses as driven by these limiting hydrogen burn conditions and spark source location assumptions. The following information provides descriptions of contents in Appendices A, B, and C.

1.1.   Summary of Appendix A

This section is the original "baseline reference" 1.25*MEB burn case analysis, which derived a peak pressure of 4.35 bar (63.1 psia) with 100% vent-flow area through the MPR. This portion of the work describes a majority of the finite-element modeling details and assumptions and structural response results for a P-T history based on a spark ignition source location at the waste surface. The basis for the P-T history was the original HMS/TRAC burn analysis and gas compositions. The current burn conditions have changed; however, the resulting structural results for the 1.25*MEB burn case remain bounded by the original analysis. Therefore, the original analysis remains as the baseline reference case and is presented herein to discuss the structural analysis methods, results, and conclusions.

1.2.   Summary of Appendix B

This section is a continuation of the original work contained in Appendix A that provides additional analysis results from modifications to HMS/TRAC P-T history. The modifications primarily are based on current knowledge of gas compositions and alternative assumptions of potential spark ignition source locations. The results for Appendix B burn scenarios are based on a spark ignition source located at the dome apex. The burn gas volume is iterated to find a structural solution that is bounded by the results presented in Appendix A. The size of the gas release then becomes the new MAB burn based on conservative estimates of gas compositions and gas release rates.

Results first are presented for the conservative-estimate gas composition, maximum expected GRE burn case having a 10,480-ft^3 gas release volume. This particular numerical analysis resulted in an unsuccessful structural solution but is maintained in this appendix for historical purposes to show that an MAB numerically must be less than an MEB.

Furthermore, given the possibility of having virtually no vent flow through the MPR, two separate GRE burn volumes have been determined to satisfy the structural integrity of Tank 101-SY. The new MAB has been found to be a 9300-ft^3 gas release volume, producing a 3.92-bar (56.8-psia) peak pressure assuming a 100% vent-flow area through the MPR. The second MAB solution is for an 8654-ft^3 GRE burn producing a peak pressure of 3.95 bar (57.3 psia) based on 0% vent-flow area through the MPR.

The analysis details and results of Appendix B complement the baseline reference analysis of Appendix A.

1.3.   Summary of Appendix C

This section provides results for two cases based on a best-estimate MEB burn having a 10,480-ft^3 GRE. The first case is based on a 100% vent-flow area through the MPR that produces a peak pressure of 3.725 bar (54 psia), and the second is based on 0% vent-flow area producing a peak pressure of 3.93 bar (56.9 psia). The major difference with these gas burn events, in comparison to Appendix B, is that the GRE is based on a best-estimate gas composition and gas release rates (specified in Ref. 1) that produce a relatively slower pressurization rate.

2.0.   ANALYSIS METHOD

The structural responses of the tank to accidental hydrogen burns was determined with the ABAQUS finite element code. The finite element structural model was adapted from one developed by WHC.[4] The basic model is documented thoroughly in the referenced report and its appendices and is not described in detail herein. Only changes that have been made to the model for application in this report are described.

The major change was to the method of describing pressure loads acting on the structure. WHC included a burn model as a user subroutine in the ABAQUS code to calculate the internal pressures. We used the pressures that were calculated by HMS/TRAC and were modified by the change in the air volume of the primary tank. The modification was simply to multiply the supplied pressures by the ratio of the original air volumes (used by HMS/TRAC) to the air volumes (calculated by ABAQUS). The effect was that the applied pressures were lowered slightly.

Other changes involved updating the fluid level and concomitant hydrostatic pressures and masses to be consistent with the best current estimates of the liquid waste characteristics[5] shown in Table 1.

The method of modeling the refractory concrete between the base of the primary tank and the secondary tank liner was modified. WHC modeled this layer as a linear material that would not crack. This material is probably already cracked and, if not, would crack very easily if the secondary tank liner were lifted by the internal pressures.

TABLE 1
LIQUID WASTE CHARACTERISTICS

Material	Specific Gravity	Depth
Slurry	1.71	0.7 m (18 in.)
Slurry	1.66	4.3 m (172 in.)
C Layer	1.54	5.3 m (210 in.)

Consequently, we modeled this material with nonlinear springs that give the material compressive strength but no tensile strength. The effect would be to cause less strain in the lower corner area of the secondary tank liner as the tank uplifts.

Another change involved fixing the lumped masses (that represent the soil on top of the dome) to the dome. WHC modeled these as separate mass lumps attached to the dome with nonlinear springs that would take no tension. In the WHC model, each mass lump could move independently of the others, which was considered unrealistic. A comparison of the two methods used for representing the soil was performed with the Los Alamos National Laboratory (LANL) tank model. This comparison showed that with either method of attaching the mass to the dome, the peak velocity before soil separation was approximately the same (within 10 to 20%).

WHC used a proprietary concrete material model to represent the concrete in the dome and cylinder of the tank. Because we did not have access to their model, we used the standard ABAQUS concrete model. Differences caused by using these models are well documented in Ref. 4.

The plastic stress-strain curve for the steel rebar was changed slightly to alleviate stability problems with the surrounding concrete cracks. This involved simplifying the curve description to eliminate a short, almost flat, section. Figure 2 shows the original stress-strain curve for the rebar, as well as the modified curve. It also shows the stress-strain curve used to model the steel liners.

The tank response to a hydrogen burn is sensitive to the coefficient of friction between the concrete cylinder and the surrounding soil. A high coefficient of friction results in minimum tank uplift but maximum hoop strain in the primary tank side wall and maximum damage in the tank dome area (concrete and attached liner) during the pressurization phase of the burn. A lower coefficient of friction results in maximum uplift of the dome but lower strain in the primary tank side wall and less damage to the dome from the initial pressure rise. However, the maximum vertical velocity is higher for this condition and results in maximum impact loads when the soil and above-tank structures separate and subsequently impact the dome as they are accelerated downward under the influence of gravity.
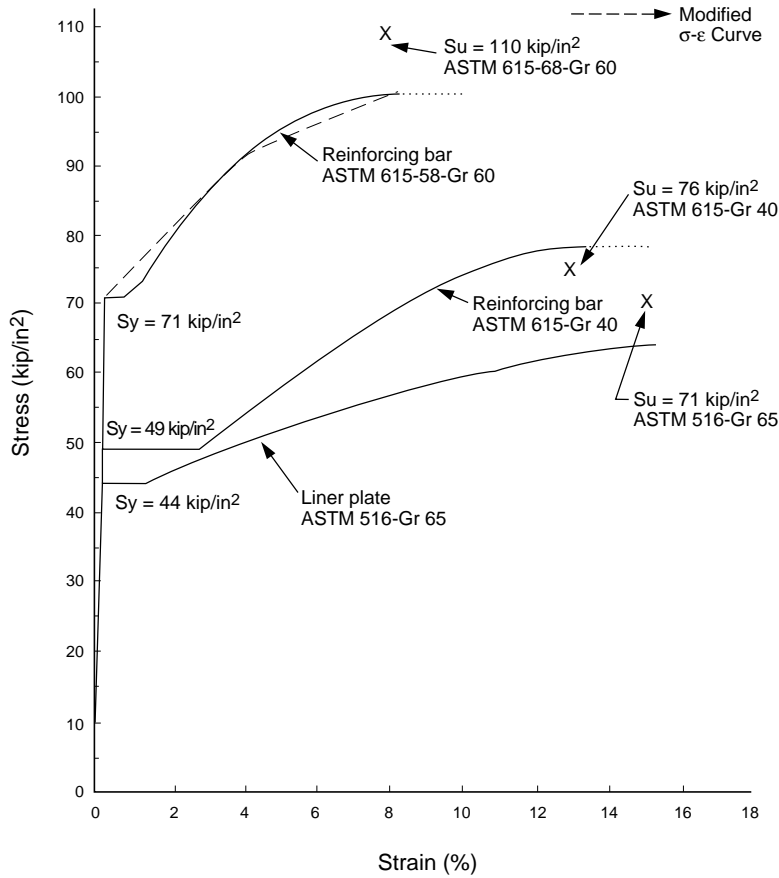
Fig. 2.   Stress-strain curves for steel liner and rebar showing changes to the grade 60 rebar curve for LANL analyses.

This uplift also could have adverse consequences on either personnel or equipment located directly above the tank. For the analysis reported here, a best estimate of the coefficient of friction of 0.57 was used. This is the same value described in the WHC report.[4]

The actual resistance to upward motion of the tank is probably somewhat higher than the resistance that results from the friction formulation used in the ABAQUS model. An additional constraint results from the forces necessary to fail the soil above the dome haunch region in a shear mode as the tank rises. This process could not be represented with the model because the soil is not explicitly modeled.

APPENDIX A

1.25*MEB PRESSURE-TIME HISTORY BURN FOR A CONSERVATIVE ESTIMATE GAS COMPOSITION WITH A WASTE SURFACE SPARK SOURCE

1.0. INTRODUCTION

As stated in the introduction, this portion of the tank structural analysis relates to a 1.25*MEB burn case having a spark source location at the waste surface. This work is retained for historical value and because the 1.25*MEB surface burn is a baseline reference analysis. The 13,100-ft^3 GRE volume, or 1.25 times greater than an MEB of 10,480 ft^3, was determined initially as the MAB. These data were included in the Safety Assessment[1] before the mixer pump was installed. However, changes in the gas composition and spark ignition location resulted in a subsequent lowering of the MAB. Therefore, the original analysis remains as the baseline reference case and is presented herein to discuss the structural analysis methods, results, and conclusions.

1.1. Tank Response to Hydrogen Burn

The tank responses are described for the limiting burn accident case with an inoperable ventilation system and a single 42-in. riser unbolted. Other parameters that define the original baseline reference case 1.25*MEB are described in Refs. 2 and 3.

Several locations on the tank structure are referenced in the following sections of this appendix. Figure 3 shows the locations of interest. The parameters associated with these locations are defined as they are used in the text.

In the figures that follow, the starting time is at 200 s relative to the pressure history that was calculated by HMS/TRAC. The data are strictly appropriate only up to the approximate time that the soil leaves the top of the tank, at which time an additional 48.3 kPa (7.0 psi) effectively is added internal to the tank. This pressure is roughly equivalent to the downward pressure of the soil and above-tank structures at the apex of the dome. The method of accounting for this increase in effective pressure is discussed later in this document.

Figure 4 shows the pressure histories (absolute) inside the tank for the 1.25*MEB case analyzed. In the figure, the higher pressure curve represents the predicted pressure in the primary tank, assuming compression of the liquid waste and constant structural volume. The maximum pressure is 436.4 kPa (63.3 psi). The next curve (dashed lines) shows the pressure in the primary tank corrected for the structural volume expansion of the tank during the hydrogen burn. The peak pressure drops ~13.8 kPa (2.0 psi) because of the structural expansion of the primary tank. The lower curve is the pressure in the tank annulus. This pressure is caused by the reduction in volume of the annulus.

Figure 5 shows the vertical displacements of four points on the tank primary liner. The locations are (1) at the apex of the dome, (2) near the top of the primary cylindrical liner, (3) near the middle of the primary cylindrical liner, and (4) near the bottom of the tank. The maximum vertical displacement of the apex is 0.389 m (15.3 in.). The bottom of the tank raise is ~0.038 m (1.5 in.) more than the top location. The middle location is about halfway between them. The vertical displacements on the three locations on the cylindrical portion of the primary liner indicate that this part of the liner shortens.

Figure 6 shows the vertical displacements of two locations on the reinforced concrete structure. The locations are (1) the apex of the dome, and (2) near the joint between the concrete cylinder and the bottom of the tank. The vertical displacement of the bottom of the concrete cylinder is less than at the apex. Most of this difference is caused by bending in the dome.

Figure 7 shows the radial displacements of two locations on the tank's primary liner. The locations are near the top and the middle of the primary cylindrical liner. The maximum radial displacement is ~0.198 m (7.6 in.), which is about one fourth of the distance across the tank annulus. Most of this deflection is plastic; therefore, the tank would remain deformed. The motion of the top location is much less than the middle location because of the support being provided by the curvature of the primary liner.
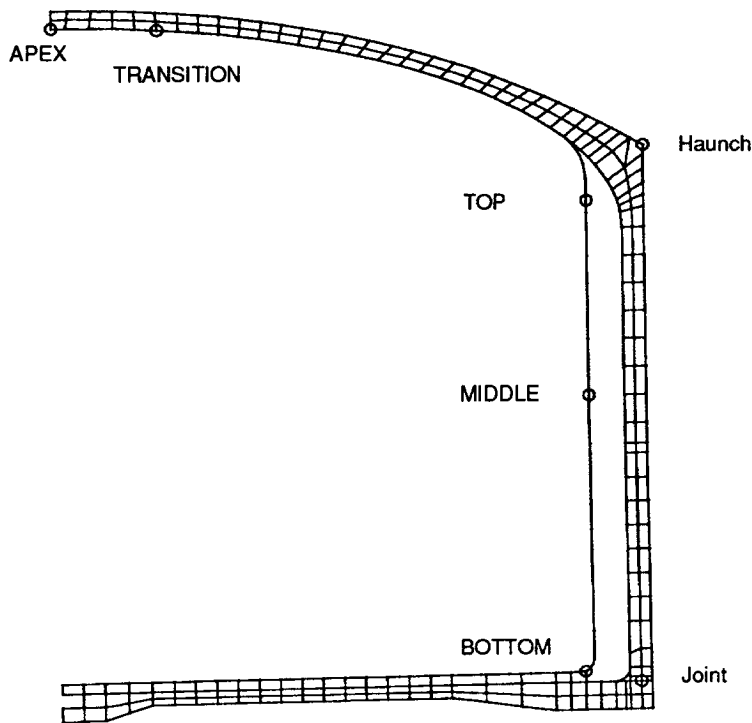
Fig. 3. Definition of locations on the tank.

MAXIMUM EXPECTED BURP — ONE RISER OPEN
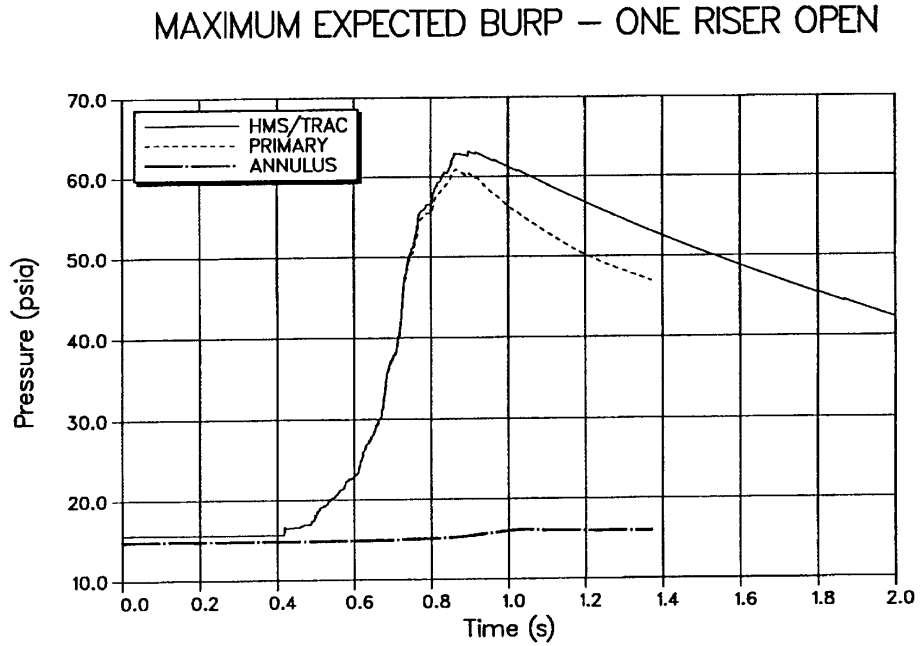
1.25 * MEB　　　　　　　　　　　　　　　　　**PRESSURE**

Fig. 4. Pressure history in tank.

MAXIMUM EXPECTED BURP — ONE RISER OPEN
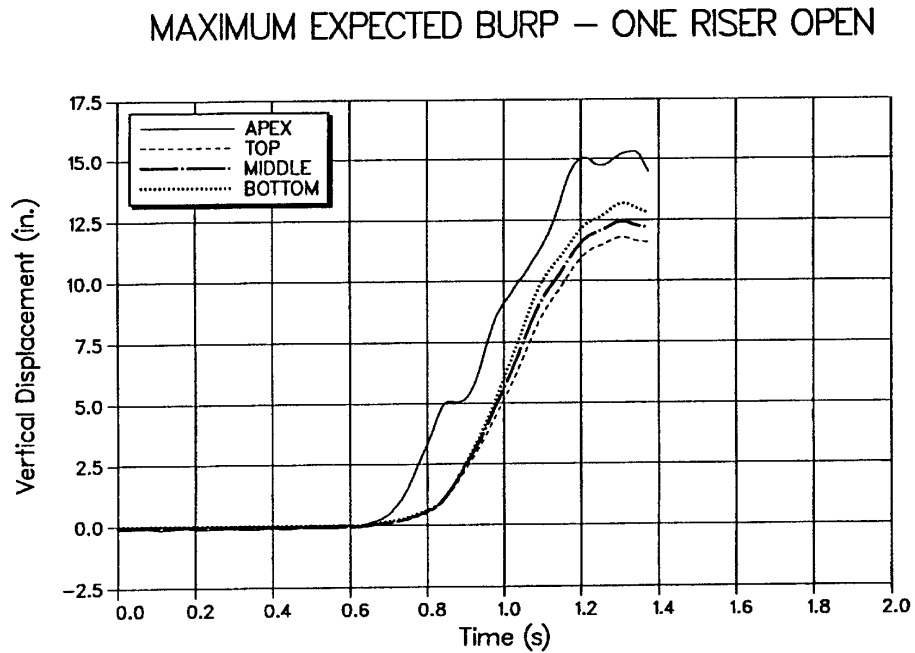
1.25 * MEB　　　　　　　　　　　　　　　　　**DISPLACEMENT**

Fig. 5. Vertical displacements of selected locations on the primary liner.

MAXIMUM EXPECTED BURP — ONE RISER OPEN

1.25 * MEB   **DISPLACEMENT**
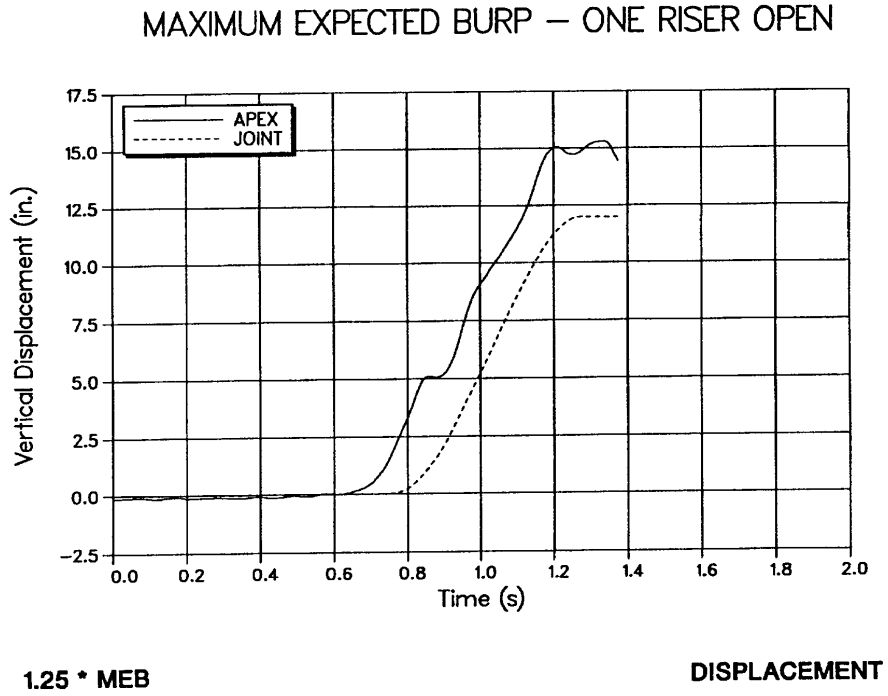
Fig. 6. Vertical displacements of selected locations on the concrete structure.
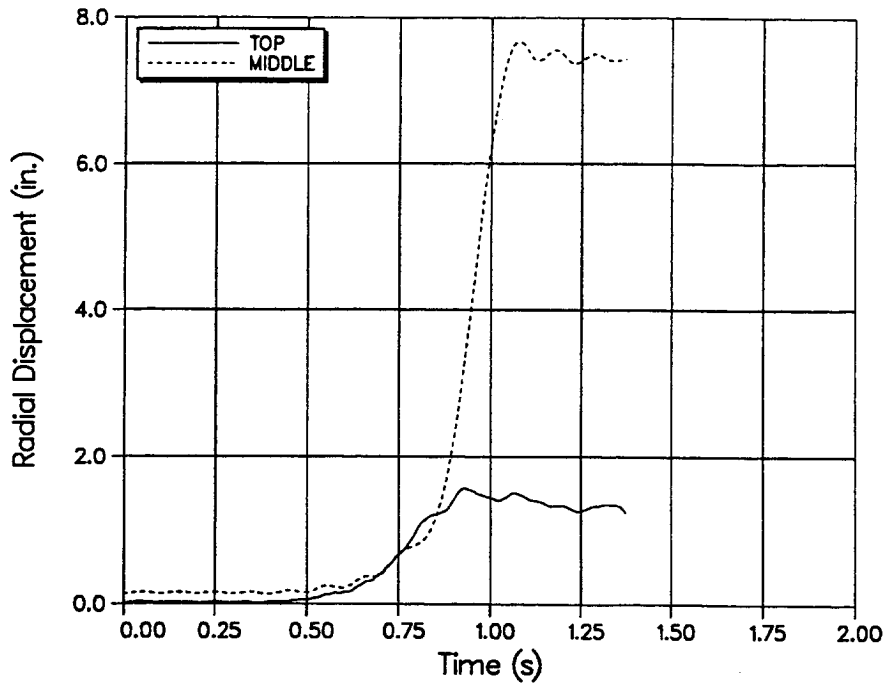
Fig. 7. Radial displacements of selected locations on the primary liner.

Figure 8 shows the changes in the volumes of the primary liner and the annulus with time. The maximum volume change is 169.9 m^3 (6000 ft^3). The maximum change in the volume of the annulus is 56.1 m^3 (1980 ft^3). These curves confirm that the maximum response of the structure had been reached.

Figure 9 shows the original and deformed shape of the tank near the end of the dynamic analysis (1.3418 s). The maximum deflection of the primary tank side wall can be seen easily. The maximum vertical displacement occurs at the apex. The failure of the refractory concrete can be seen in the lower outside corner of the secondary liner.

The most important parameter in terms of tank leakage is the strain of the primary steel tank. We have used the same strain criteria that WHC used in their report.[4] Strain limits are calculated based on the expected uniaxial strain limit for the tank material. This limit then is reduced based on the calculated stress state in the material. The calculated global membrane strain then is multiplied by strain concentration factors that depend on the type of discontinuities present and is compared with the limit strain. Strain concentration factors are estimated based on the WHC report and information from an Electric Power Research Institute report.[6] In the following analyses, these factors are given a range of values because they are not directly applicable to this situation.
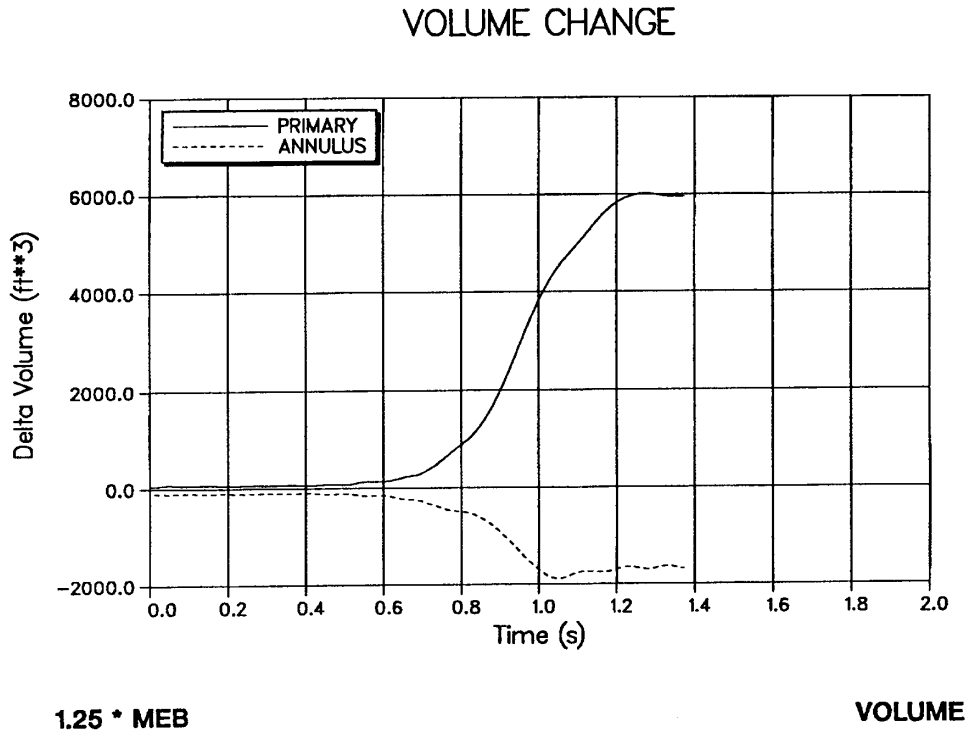
Fig. 8. Change in volume of the primary liner and annulus.
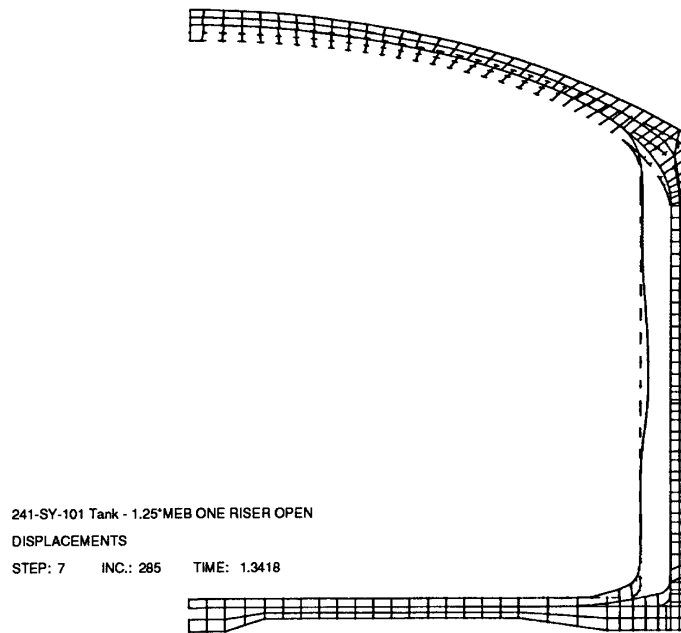
Fig. 9. Deformed shape of the tank.

The tank membrane strains must be considered in several locations, including the primary tank and secondary tank liners below the fluid level, the primary liner in the dome region, and the concrete reinforcement. Review of the finite element model results indicates that only three locations in the structure needed to be evaluated: the primary tank wall at the maximum deflection below the liquid level, the primary liner in the dome near the thickness transition, and the rebar in the dome near the liner thickness transition.   All other locations experienced low enough strain that they are not of concern.

Figure 10 shows the meridional and hoop strains in the primary tank side wall at the location where the maximum radial displacement occurs. The largest strain in the side wall is <0.016. When this hoop strain is maximum, the meridional strain is negative. Therefore, the limit strain is equal to the uniaxial ultimate strain for the tank material, which is 0.27.[1] The margin to failure for the primary tank wall below the liquid level is 16.8 and therefore is of no concern.   Figure 11 shows the meridional and hoop stress for this location. The meridional stress is very low; however, the hoop stress exceeds the yield strength of the material.

On the dome, at a radius of ~1.83 m (72 in.) from the tank's center line, the liner thickness changes from 12.7 to 9.53 mm (0.5 to 0.375 in.). This location is the weakest in the dome because the meridional reinforcement in the concrete also makes a transition at about the same tank radius. The effective rebar cross-sectional

13

area changes by a factor of two because every other rebar is stopped at a tank radius of 2.21 m (87 in.). The radius of the thickness transition, 1.83 m (72 in.), is also the location of a 0.10-m (4-in.) penetration (penetration 15a). The thickness transition bisects the penetration.

To evaluate the safety of the tank at this location, the strains, stresses, and vertical velocity of the dome are needed. Figures 12 and 13 show the computed meridional and hoop strains for the dome region near the liner thickness transition. Strains are given for the liner, inner rebar, and outer rebar. Figures 14 and 15 show the computed meridional and hoop stresses in the liner, inner rebar, and outer rebar at the transition. Figure 16 shows the vertical velocities for three locations on the dome: the apex, transition, and haunch.

The procedure established to evaluate the safety of the tank requires that the strains in the liner be corrected to account for the additional strains expected when the soil and above-tank structures separate from the top of the dome. These additional strains have been approximated in the following manner. First, the maximum vertical velocity of the dome with soil and structures attached is obtained from the ABAQUS model predictions. Using this velocity, the maximum separation of the dome and soil is calculated using the relationship between initial velocity and maximum rise height in a **1-g** environment. Because the dome is moving downward at the time of separation, only a portion of this separation can contribute to additional strains. This portion has been approximated to be one-half of the separation distance at the apex. This value is assumed to be the change in radius and then is divided by the approximate instantaneous radius of the dome (obtained from the ABAQUS model) to calculate the additional strains.

Because failure of the tank for this burn case would initiate at the thickness transition in the dome of the tank, a detailed description of the failure criterion that has been used is needed. This failure criterion is thought to be somewhat conservative, and the associated parameters discussed below will be determined more accurately when additional planned analyses are completed.

If the numerically calculated strain (from the ABAQUS code) in the 3/8-in.-thick section of the dome liner exceeds ~1.0%, the liner is expected to tear where a 4-in.-diam penetration passes through the transition. Thus, local tearing occurs for this burn case. Given that a tear exists in the liner near the penetration, it is critical to determine whether the tear propagates. According to a modified version of the net-section stress criterion,[7,8] a crack will propagate if the net-section stress in a plate with a through crack exceeds a value that is called the critical flow stress.

MAXIMUM EXPECTED BURP — ONE RISER OPEN
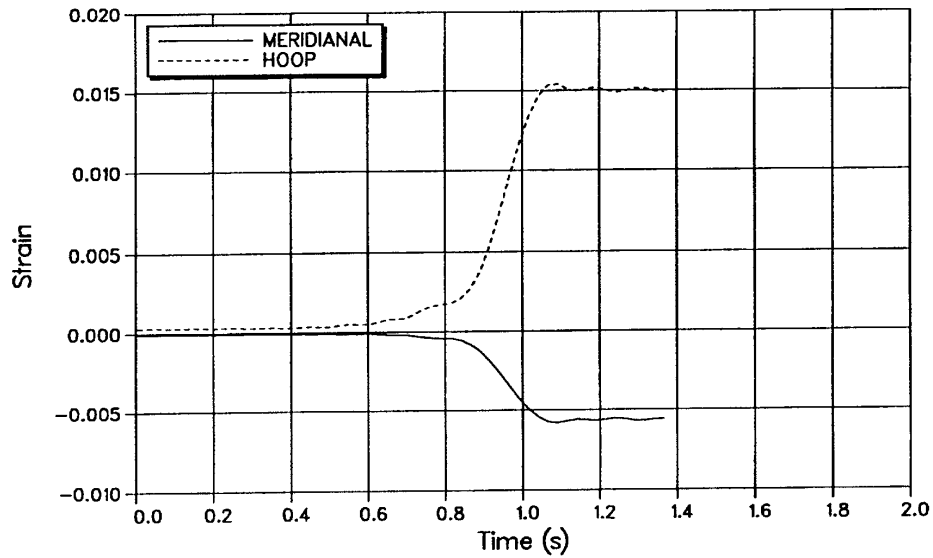
1.25 * MEB   **MIDDLE**

Fig. 10. Strains in the primary liner near the middle of the tank.

MAXIMUM EXPECTED BURP — ONE RISER OPEN
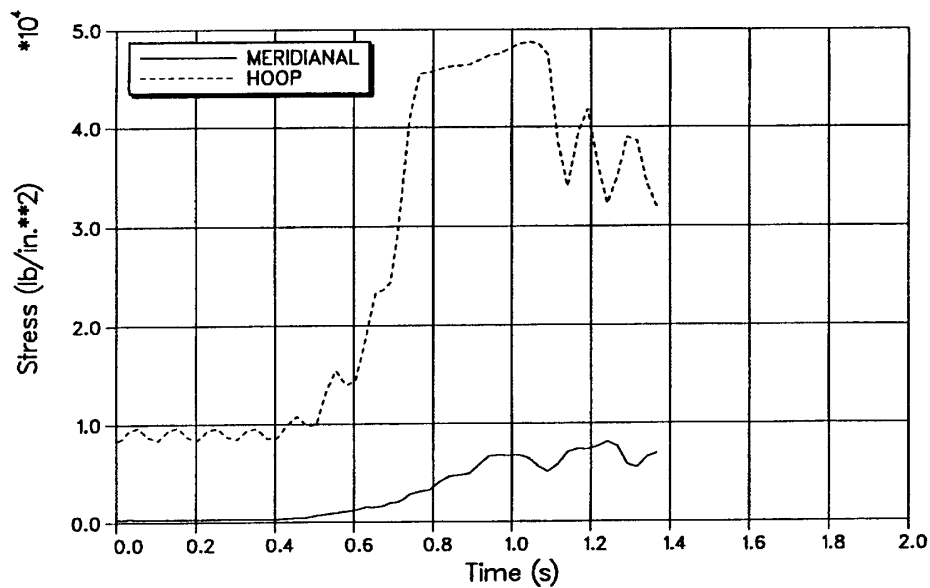
1.25 * MEB   **MIDDLE**

Fig. 11. Stresses in the primary liner near the middle of the tank.

15

MAXIMUM EXPECTED BURP — ONE RISER OPEN
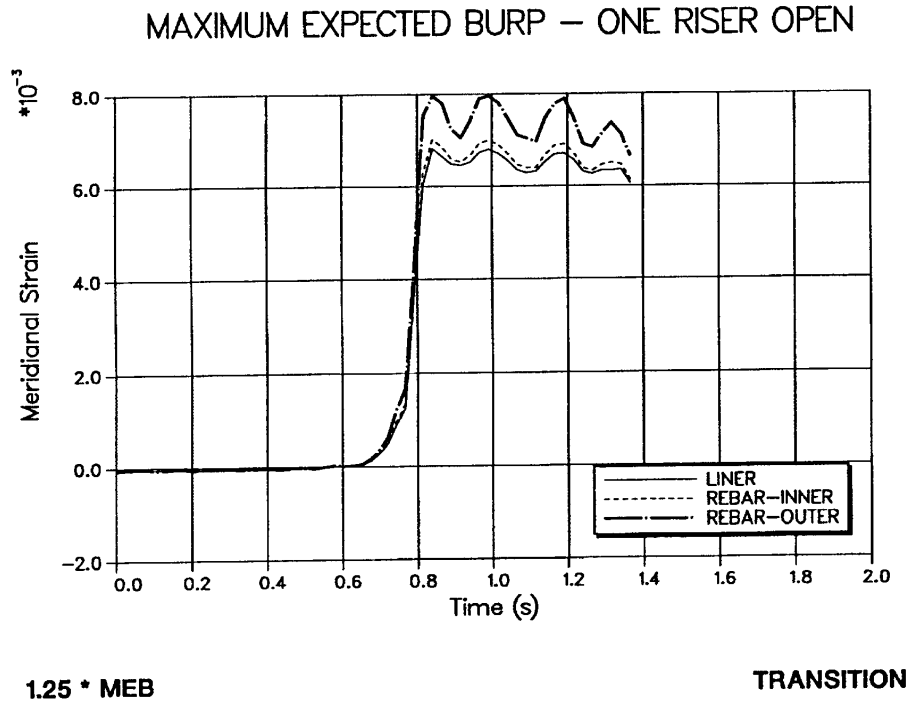
1.25 * MEB   **TRANSITION**

Fig. 12. Meridional strains at the transition location.

MAXIMUM EXPECTED BURP — ONE RISER OPEN
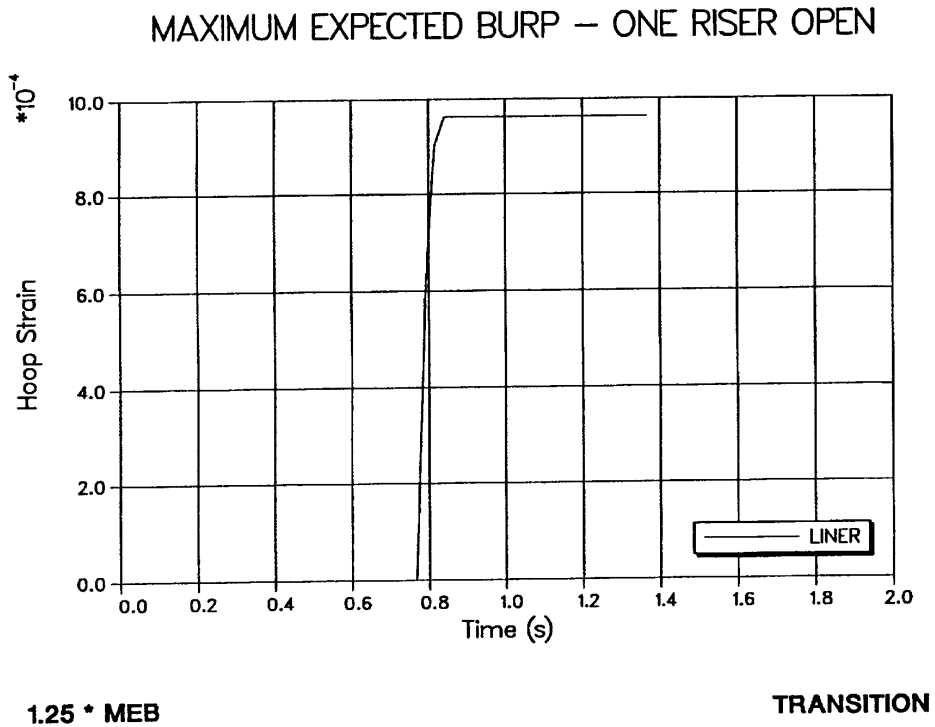
1.25 * MEB   **TRANSITION**

Fig. 13. Hoop strain in the liner at the transition location.

16

MAXIMUM EXPECTED BURP — ONE RISER OPEN
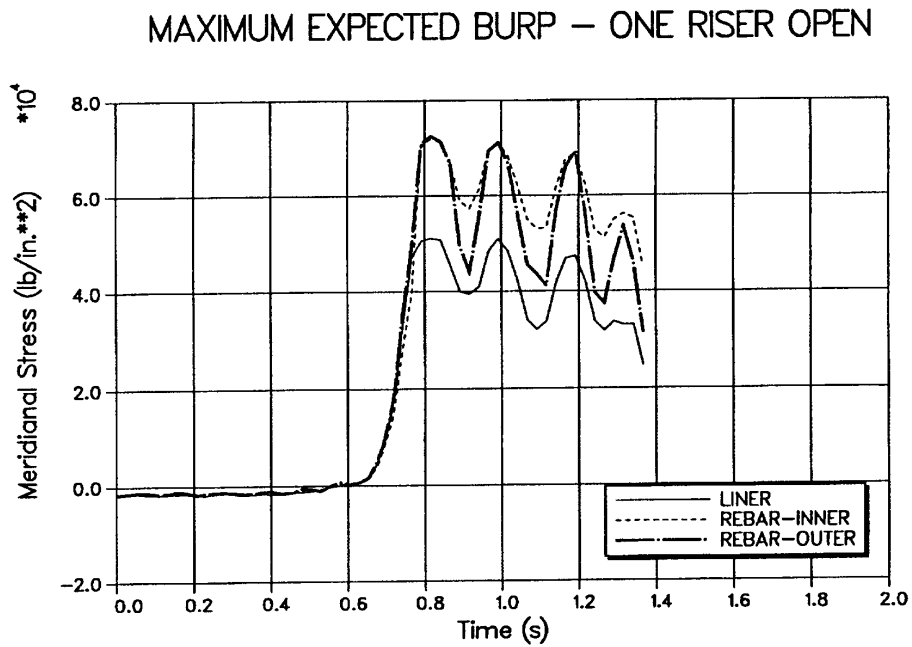
1.25 * MEB   **TRANSITION**

Fig. 14. Meridional stresses at the transition location.

MAXIMUM EXPECTED BURP — ONE RISER OPEN
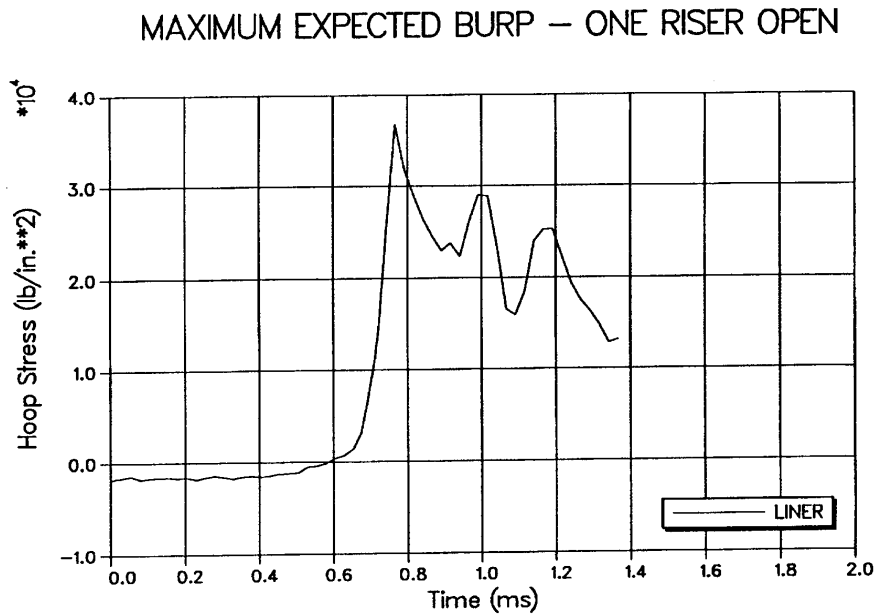
1.25 * MEB   **TRANSITION**

Fig. 15. Hoop stress in the liner at the transition location.

17

MAXIMUM EXPECTED BURP — ONE RISER OPEN
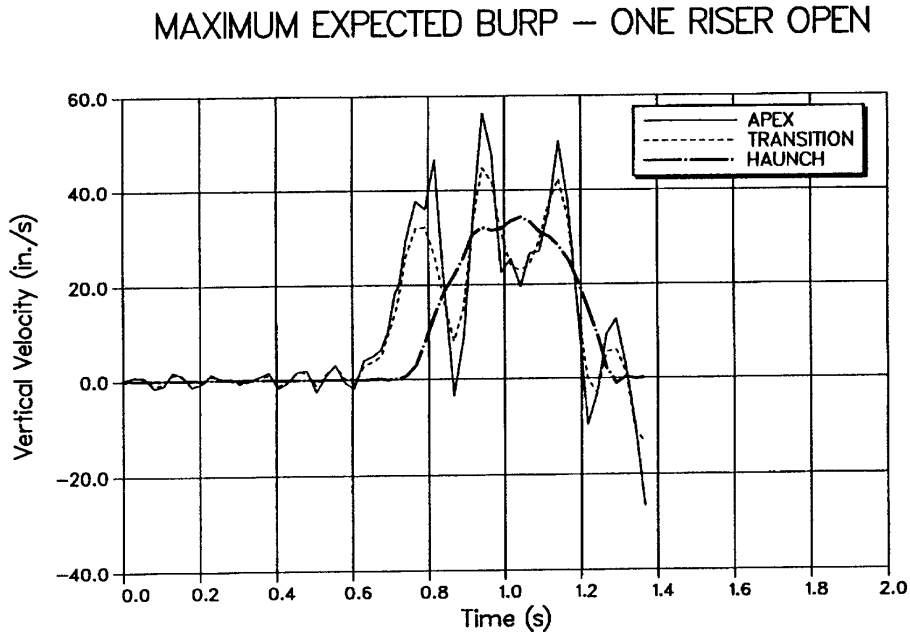
1.25 * MEB   **DOME**

Fig. 16. Vertical velocities at selected locations on the dome.

The critical flow stress usually is taken to be the average of the material yield and ultimate strengths unless specific tests have been performed to measure critical flow stress values. Using typical values for yield and ultimate stresses from the WHC report,[4] the critical flow stress (true stress) would be 409 MPa (59.5 ksi). The failure criterion including the critical flow stress is discussed further in Ref. 9.

Also included in Ref. 9 are the calculations associated with the tearing of the liner around the penetration. When the corrected strains for the separation of the soil, strain concentration factors for the thickness transition, and penetration are included, the calculated stress is 401 MPa (58.3 ksi). This value is less than the critical flow stress given above. Therefore, the tear in the liner will not propagate.

The response of the tank to the impact of the soil and structures that are located on top of the tank dome is difficult to determine and has been estimated as follows. A failure analysis of the dome indicates that ~2.6 x 10^{7} in.-lb of energy can be absorbed in the reinforcement in the haunch region before the dome would fail catastrophically. Because that much energy can be absorbed, the total mass on top of the dome could be dropped by as much as 0.0098 m (3.85 in.). To achieve this height, the vertical velocity of the dome would have to exceed 1.38 m/s (54.5 in./s). The velocity at the transition location of the dome, plotted in Fig. 16, was used to approximate the upward velocity [1.14 m/s (45.0 in./s)] of the material above the tank. Based on this method, it is predicted that the dome probably would survive

18

this soil impact. Details of the assumptions and results are presented in Refs. 10 and 11.

A second dome failure mode caused by impact of the soil and above-structures must be considered because of the possibility of severe damage to the dome near the thickness transition of the liner (see above). If the liner tears around the thickness transition, the rebar alone at this location would have to absorb the impact of the soil and above-tank structures, which consist primarily of the pump pit and, if attached, the pump. As described earlier, the rebar could be strain-hardened significantly or even fail during the pressure rise portion of the burn, which may leave little capacity for absorbing the impact loads. Our best estimate is that if the liner tears during the pressurization portion of the burn, the dome would fail at this point, allowing the pump pit structure to fall into the tank. Because a large tear in the liner was not predicted, this mode of failure should not occur.

APPENDIX B

MAB BURN TRANSIENT FOR A CONSERVATIVE-ESTIMATE GAS COMPOSITION AND DOME SPARK SOURCE LOCATION

1.0   INTRODUCTION

This section focuses on the structural response of Tank 101-SY to a hydrogen burn having a spark source located in the ventilation system directly under the dome. The gas composition is a conservative estimate of expected results and is slightly different than the original baseline reference case. However, the conservative composition of gas by itself has little effect on the structure. In this scenario, the burn initiates just under the dome, trapping more fuel rather than forcing unburned gases through the vent.

1.1.   Comparison of 1.0*MEB & 1.25*MEB Burn Pressure Transients

The original baseline-reference P-T history for the 1.25*MEB burn (13,100-ft^3 gas volume) analyzed in Appendix A is shown in Fig. 17. The peak pressure is ~4.35 bar (~63.0 psia). Figure 18 shows the conservative gas composition P-T history for the 1.0*MEB case having a 10,480-ft^3 gas volume and reaching a peak pressure of 4.15 bar (~60.0 psia).

A comparison of these curves shows that the P-T history at the beginning of the transient, for the new burn case shown in Fig. 18, is much higher than the original baseline reference case of Fig. 17. Table 2 gives a comparison of the pressure-rise time and the rate of pressurization (dP/dt) for both cases, calculated from 1 bar to peak pressure. These values are taken from the point where there is pressure initiation after 1 bar atmospheric to the maximum peak pressure, and they should be viewed in a qualitative sense. The table merely represents the large difference between pressure rates. However, the actual rate of pressurization for the original case in Fig. 16 is much slower than reported above because the slope is constantly changing. That is, the original P-T history curve has a gradual buildup over a longer time increment. In effect, it depicts a "slow" pressurization case, which does not exhibit a definite straight-line relationship. It nevertheless has a "semilinear" portion occurring at ~0.6375 to 0.7625 s. However, this linear portion results in a dP/dt of ~200 psia/s.

TABLE 2
COMPARISON OF PRESSURE RISE TIMES
AND RATE OF PRESSURIZATION

Pressure Curve	Rise Time (Δt)	Pressure Rate (dP/dt)
Original 1.25*MEB	0.482 s	98.7 psia/s
Conservative 1.0*MEB	0.234 s	194.4 psia/s

HMS/TRAC Pressure-Time History
1.25*MEB Burn 13,100 ft^3 GRE
HLW Tank 101-SY
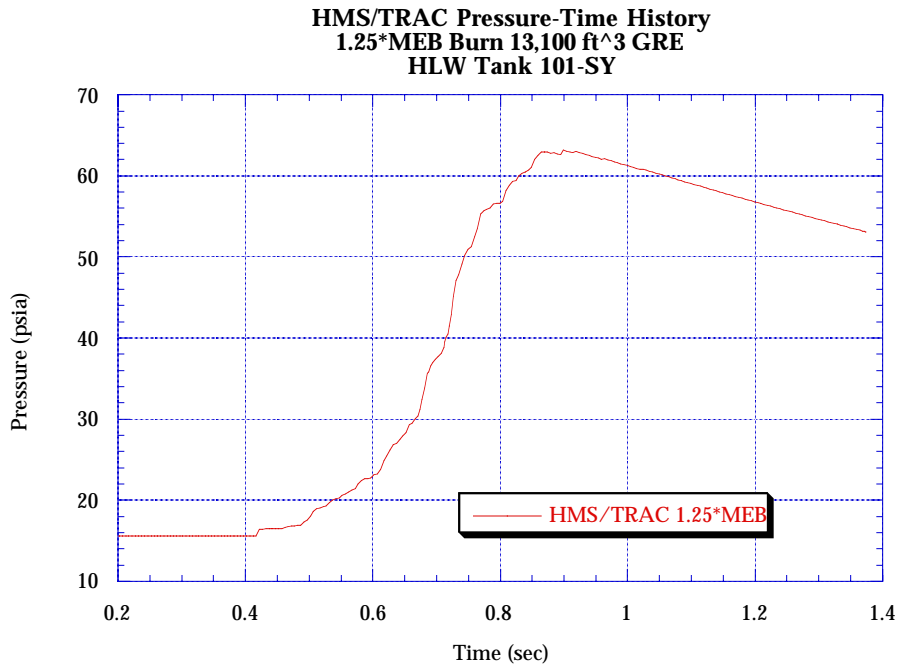
Fig. 17. P-T history for original 1.25*MEB burn case spark source at waste surface.

HMS/TRAC Pressure-Time History
1.0*MEB Burn Case - 10,480 ft^3 GRE
HLW Tank 101-SY
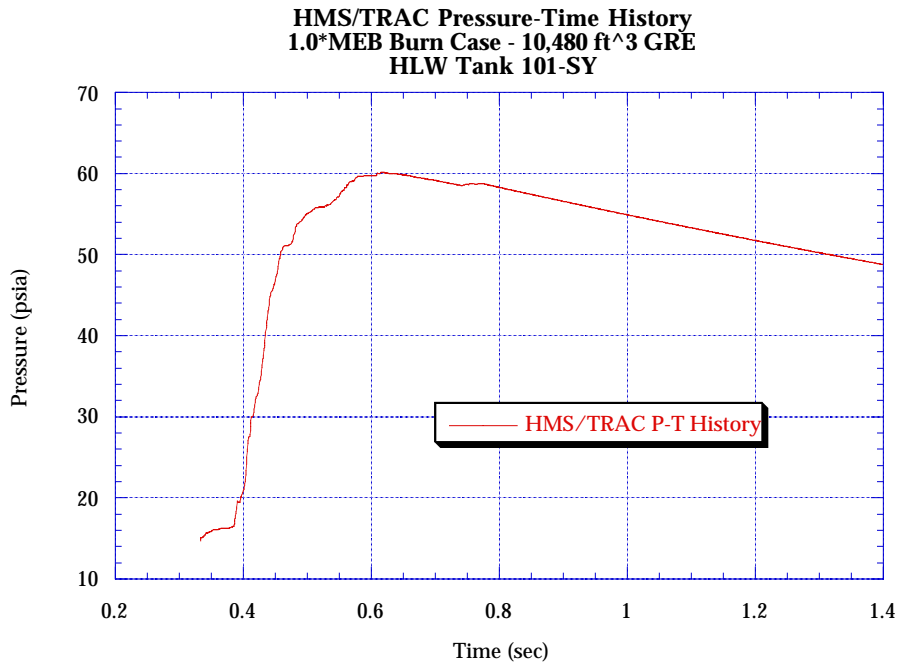
Fig. 18. P-T history for new MEB burn case spark source at underside of dome.

Conversely, the curve of Fig. 18 has a markedly higher rate of pressure rise, being almost linear through the initial 0.12 s of the transient, then gradually decreasing until the pressure reaches 4.15 bar (~60 psia). The rate of pressurization in this portion of the curve, i.e., the change in pressure with respect to time dP/dt, is ~490 psia/s, which is approximately five times the original 1.25*MEB pressure curve, or ~2.5 times the linearized portion of Fig. 17. In effect, the 1.0*MEB P-T history is considered a "fast" pressurization. In comparison, this effect creates an equivalent "impact" loading on the structure that has not been seen or addressed previously. The main point of this comparison is that the relatively larger rate of pressurization for the 1.0*MEB case creates a significant difference in the overall response of the tank dome.

1.2. Tank Response to 1.0*MEB Hydrogen Burn

Several iterations of the 1.0*MEB top-side burn case were performed with no apparent numerical solution to the structural response of the tank throughout the complete burn transient. The numerical solution within the ABAQUS code failed successively just after the program reached the peak pressure, and the dome's apex velocity-time history showed a downward trend, as depicted in Fig. 19. The dome velocity at this peak pressure, just before the program failed, showed much higher velocities than the original baseline reference 1.25*MEB burn for a waste surface spark source. However, it is not clear whether this peak velocity is the "true" peak or a secondary peak.

For example, as Fig. 16 shows for the original 1.25*MEB case, the first velocity peak is not the highest. There are actually three major velocity peaks, with the second being the maximum. Therefore, because of the numerical difficulties encountered with the 1.0*MEB case, we cannot ascertain whether the velocity peak of Fig. 19 is the highest.

From Appendix A of this document, we concluded that the peak dome velocity for the 1.25*MEB surface burn case should be >54.5 in./s to cause dome failure from reimpaction of soil above the tank. Consequently, as shown in Fig. 19, the peak velocity of 68 in./s is much higher than would be allowed to preclude dome failure. Therefore, dome failure is expected during this transient based on the higher peak velocity.

Conceivably, there may be a velocity peak >68 in./s if the transient solution progressed.

Figure 20 shows the dome velocity as a function of position from the apex. This plot clearly shows that the dome apex velocity is much higher than the haunch region.

Velocity-Time History Dome Apex
1.0*MEB Burn 10,480 ft^3 GRE
HLW Tank 101-SY
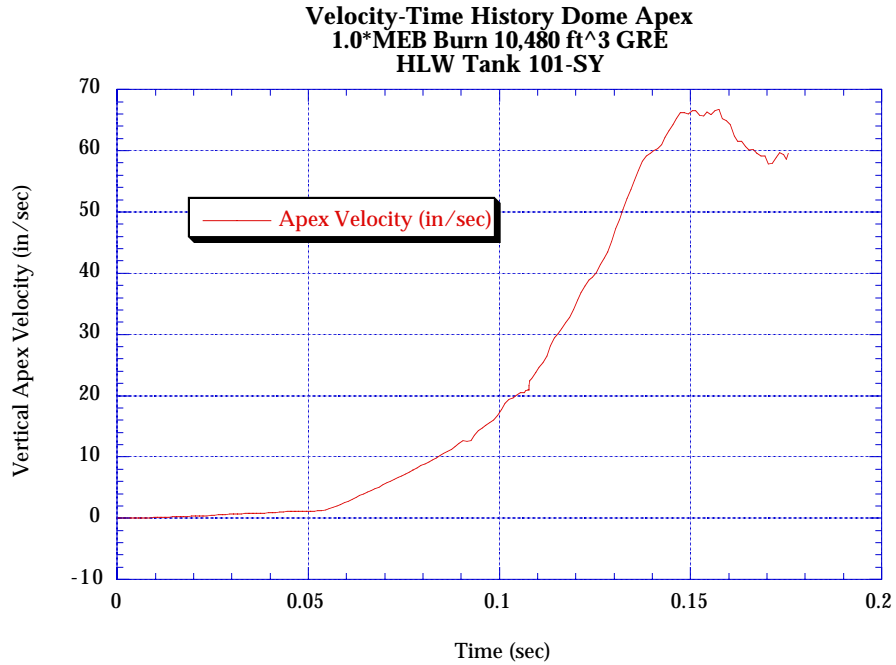
Fig. 19. Dome apex velocity at peak pressure for 1.0*MEB.

At this time point in the transient, the rest of the tank structure has not had time to respond to the applied pressure, which shows very little vertical motion everywhere, including at the base of the tank wall. Figure 21 shows the relative displacement of several selected locations throughout the tank structure. The dome's apex vertical deflection at the peak pressure is ~3.25 in., whereas the haunch and tank wall base have displaced only ~0.25 in. This constitutes a factor of 13 difference between the dome apex displacement and the tank wall bottom. The conclusion is that the dome structure is reacting extensively to an excitation. Results, findings, and conclusions of these analyses are summarized herein and are documented in Ref. 2.

As a result of the problems encountered with the numerical solution at 1.0*MEB, it was reasoned that a fundamental frequency was being excited during the pressure transient, partly because of the high pressurization (dP/dt) rate. This high rate of pressurization, combined with the peak pressure at 4.15 bar (60.2 psia), is considered to create a resonant condition, which was exhibited as a numerical instability within the ABAQUS code.

The finite element model has no structural or mass damping included to reduce the peak amplitudes. The only form of equivalent "damping" or energy dissipation is through the nonlinear effects embedded in the code, such as metal plasticity, concrete cracking, and nonlinear geometric effects.

Velocity vs Radial Distance Apex to Haunch
1.0*MEB Burn Case - 10,480 ft^3 GRE
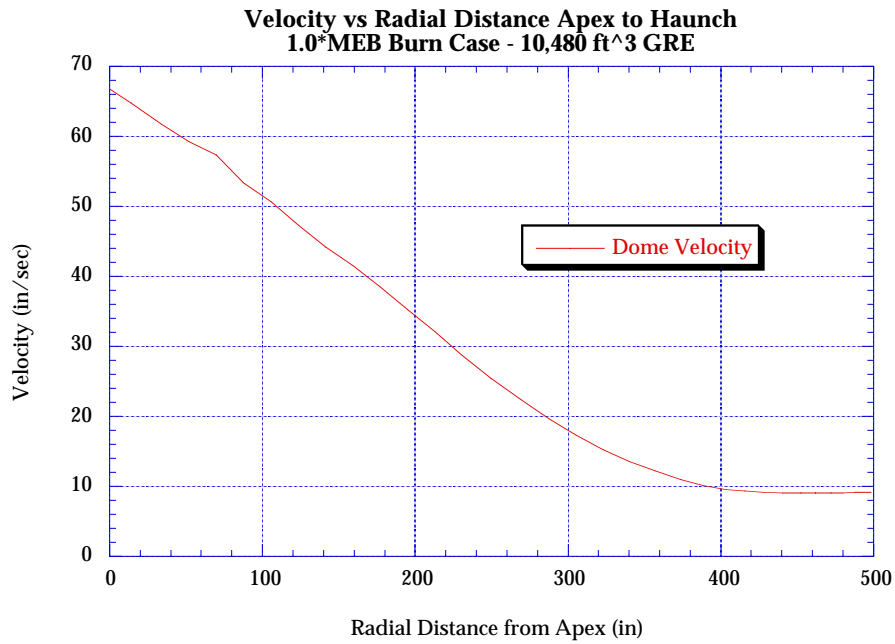
Fig. 20. Dome velocity profile vs position from apex for 1.0*MEB.

Displacement-Time History 1.0*MEB Burn
Selected Locations on HLW Tank 101-SY
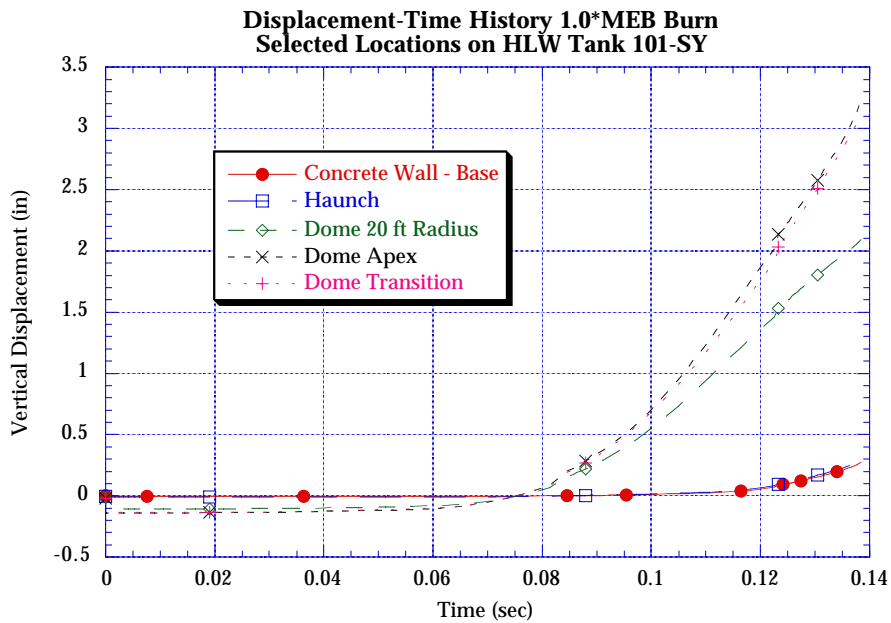
Fig. 21. Vertical displacement at selected tank location.

Furthermore, to include damping in a dynamic analysis such as this, which tends to be more like an impact loading than a slow pressurization, would not prove useful because the timespan for initial pressurization is rather short. That is, the pressurization rate (dP/dt) is very high and of short duration, and damping would not improve the response, except within the region of harmonic oscillations. To qualify this position, further confirmatory-type analyses were developed.

1.3.   Shock Response Spectrum

The structural response of Tank 101-SY, especially the reinforced concrete dome, depends on two parameters: (1) the driving frequency of the burn pressure pulse, and (2) the fundamental frequency of the structure. If the driving frequency is coincident with the fundamental frequency, given no energy dissipation such as damping, then infinite response is expected from the structure. That is, a resonance condition would ensue such that stresses, strains, displacements, etc., would go unbounded.

A response spectrum analysis provides an approach of estimating the peak response of the structure subjected to a base motion. The base motion in this case is actually the P-T history, which in effect is the forcing function. The response is assumed to be linear, thus coinciding with the frequency domain of the structure. In a simplified single-degree-of-freedom system, the equation of motion subjected to a forcing function is:

$$m\ddot{y} + ky = F(t)$$

where k is the stiffness of the structure, m is the mass, and the forcing function, F(t), could be a function such as:

$$F(t) = F_o \sin \gamma t \quad .$$

However, in this particular problem, the forcing function is merely the P-T history. The solution to the above equation of motion is given by the complementary and particular solutions of a second-order linear differential equation.

$$y(t) = y_c + y_p$$

$$y_c = A\cos \omega t + B\sin \omega t$$

$$y_p = C\sin \gamma t$$

where

ω = natural frequency of vibration of structure (rad/s),

$$\omega = \sqrt{\frac{k}{m}} = \frac{2\pi}{T} \quad,$$

T = natural period of vibration (s),
γ = driving frequency of forcing function (rad/s),

$$\gamma = \frac{\pi}{t_d} \quad,$$

t_d = period of forcing function (s),

and noting that the static deflection of the structure at a point is:

$$y_{st} = \frac{F_o}{k} \quad.$$

Solving the equation of motion in terms of y and y_{st} :

$$y(t) = A\cos\omega t + B\sin\omega t + \frac{F_o}{k}\left[\frac{1}{1-\left(\frac{\gamma}{\omega}\right)^2}\right]\sin\gamma t \quad.$$

If the initial conditions at $t = 0$ are $y(t) = 0$ and $\dot{y}(t) = 0$, then

$$\frac{y(t)}{y_{st}} = \frac{1}{1-\left(\frac{\gamma}{\omega}\right)^2}\left[\sin\gamma t - \frac{\gamma}{\omega}\sin\omega t\right] \quad,$$

and the parameter $\dfrac{y(t)}{y_{st}}$ is the amplification, or dynamic load factor (DLF) of the structure above its static deformation, caused by the forcing function $F(t) = F_o\sin\gamma t$.

A simplified shock response system (SRS) analysis, based on the conservative gas estimate 1.0*MEB P-T curve, revealed structural amplifications of 1.5 to 1.8 throughout the range of frequencies of 1 to 4 Hz. Secondly, the SRS analysis was performed with material properties in an undegraded state. Although the SRS analysis is a linear calculation over the entire frequency range and does not account for nonlinearities, it nonetheless provides qualitative results and trends.

A subsequent modal analysis of the tank structure revealed that the dome has a fundamental frequency of 7.4 Hz based on the nondegraded materials state, i.e., purely linear-elastic material behavior. Confirmatory analyses,[12] which are based on classical theoretical solutions and a finite-element method, show similar results for conditions in Tank 101-SY. However, the actual dome structure subjected to severe pressure loadings exhibits increased nonlinear effects, with extensive concrete cracking and steel rebar and portions of the primary steel liner yielding. This process may be viewed in simple terms of a single degree-of-freedom system, such that the natural frequency is proportional to the square root of the quantity of stiffness divided by mass:

where

$$f = \frac{1}{2\pi}\sqrt{\frac{k}{m}},$$

f = frequency, s^{-1} (Hz),
k =   stiffness, (lb/in.), and
m =   mass, (lb-s^2/in).

As the structure proceeds into the nonlinear regime, the flexibility of the entire system increases (i.e., the stiffness, or "k," decreases), thus decreasing the natural frequency of the structure. At each time increment throughout the pressure transient, additional material becomes nonlinear, thereby increasing flexibility incrementally. Therefore, the tank natural frequencies are changing constantly along the path of the transient. Natural frequencies calculated for a structure in a pristine state obviously would be higher than during a burn transient because of material degradation. Thus, the dome's 7.4-Hz fundamental frequency actually will be much lower as the dome's concrete cracks and the rebar and primary steel liner yield.

This behavior may be understood by applying simple stiffness reductions to a model of the tank and calculating the natural frequencies. That is, to obtain an estimate of the "reduced" fundamental frequency of the tank structure, the modulus of elasticity of the concrete was lowered artificially. In effect, this causes the flexibility to increase and the natural frequencies to decrease. Table 3 shows the fundamental natural frequency of the tank (specifically the dome) as a function of reduction in modulus of elasticity for all concrete dome elements.

TABLE 3
FUNDAMENTAL DOME FREQUENCY VS REDUCTION IN CONCRETE
MODULUS OF ELASTICITY (REDUCTION IN STIFFNESS) FOR THE DOME
CONCRETE ELEMENTS

% Reduction in Dome Modulus of Elasticity	Fundamental Frequency (Hz)
0	7.5
2.5	4.09
5	4.04
10	3.94

To obtain an estimate of the dome's fundamental frequency during the pressure transient, a modal analysis was performed just before the numerical solution of the 1.0*MEB case failed. That is, ~0.15 s into the pressure transient, the dynamic analysis was terminated and a modal analysis of the "degraded" structure was performed. At this point, the internal pressure is ~60 psia, and the tank's dome structure has sustained extensive concrete cracking and rebar yielding. Results of the modal analysis showed a fundamental dome frequency of 1.14 Hz with 99.7% of the modal weight active. As stated above, the simplified SRS showed amplification, or DLF, in the range of 1.5 to 1.8 within the frequency range of 1 to 4 Hz.

A comparison of the degraded structure's fundamental frequency for both the 1.25*MEB burn case with a spark source at the waste surface and the 1.0*MEB burn case with a spark source at the dome is shown in Table 4. Qualitatively, the table shows that amplification is higher for the 1.0*MEB burn case. Again, this must be interpreted qualitatively and not as actual. Nonetheless, comparing the amplification, we see that the ratio of DLFs for the 1.0*MEB case vs the 1.25*MEB case is ~44% higher. This implies that we should expect a higher response and subsequently, potential dome failure.

$$DLF_{(1.0*MEB)} = 1.8,$$
$$DLF_{(1.25*MEB)} = 1.25,$$
$$f = DLF_{(1.0*MEB)}/DLF_{(1.25*MEB)} \text{, and}$$
$$f = 1.44.$$

Without performing any subsequent analyses, we reasoned that a qualified and accurate numerical solution to the structural response was required based on a peak pressure less than the 1.0*MEB burn case. In other words, using the burn case for a spark source location at the underside of the dome, P-T curves were developed for several gas release volumes and corresponding peak pressures. The P-T transients then were applied successively to the structural finite element model to develop a parametric representation.

TABLE 4
FUNDAMENTAL FREQUENCIES AND AMPLIFICATION
FREQUENCY RANGE

Pressure Transient Case	Fundamental Frequency	Active Modal wt %	Amplification (DLF)
1.0*MEB Nonlinear	1.14 Hz	99.7	1.80
1.25*MEB Nonlinear	0.54 Hz	99.4	1.25

1.4. Parametric Analysis Results

Because the 1.0*MEB burn case was unsuccessful, parametric analyses were conducted to determine the conservative gas composition GRE that would satisfy the structural integrity of Tank 101-SY. Table 5 lists the numerous analyses performed for selected GRE volumes. Pertinent parameters, such as pressurization rates, gas volumes, and peak pressures, also are listed. Any reference in Table 5 to a 100% riser area should be considered synonymous with a 100% vent-flow area through the MPR.

Certain parameters were plotted from the data of Table 5, which showed very interesting correlations. Figures 22 and 23 show pressurization rates vs gas release volumes and peak pressures vs gas release volumes, respectively. The parametric data in each case were fit to a fourth-order polynomial, which now provides a basis for obtaining estimates within the ranges of applicability.

The relationship of dP/dt vs GRE volume, as shown in Fig. 22, appears representative of a "backward-S," depicting a sharp increase in pressurization rate at gas release volumes above 9500 ft^3. That is, in the region above 9500 ft^3, small increases in gas volume produce large increases in pressurization rate (dP/dt). This is seen again in Fig. 23, representing peak pressure vs gas release volume.

Figure 24 shows the peak pressure vs pressurization rate for the cases studied. The correlation for these parameters does not have a good fit. However, qualitatively we see the relationship for large increases in pressurization rate for small increases in peak pressure.
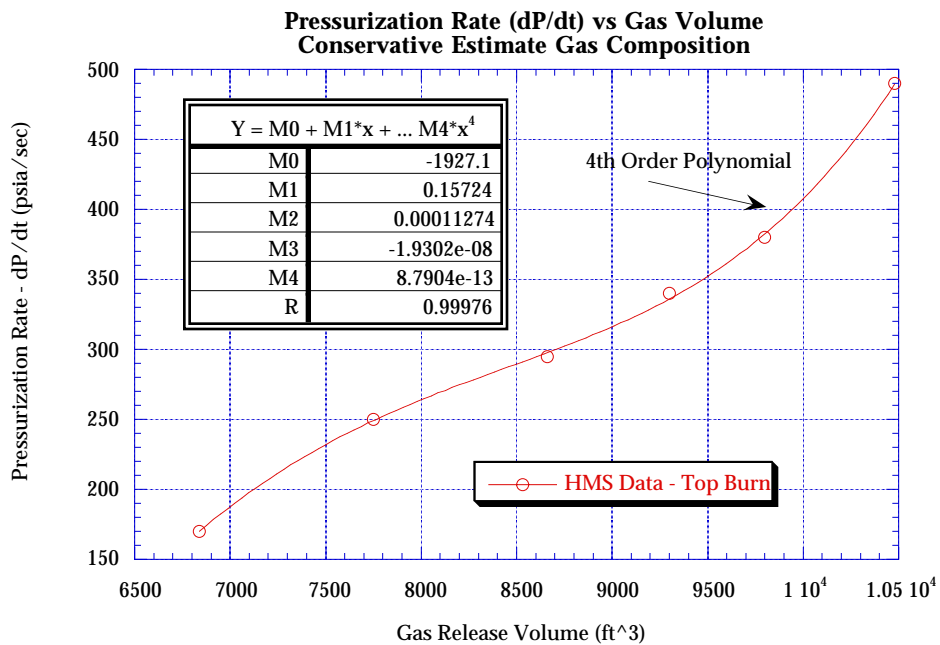
Fig. 22. Pressurization rate vs gas release volume.

TABLE 5
PARAMETERS OF BURN PRESSURE TRANSIENTS

Burn Case	Peak Pressure (psia) (bar)	Rate of Pressure dP/dt (psia/s)	Spark Location	Total Combustion Energy (Btu)	Average Flame Velocity (ft/s)	Total Gas Release Volume (ft^3)	Max. Dome Velocity (in./s)	Remarks
1.25 MEB Baseline	63.1 (4.35)	200	Waste Surface	1.09E+06	167	13,100	57	Original baseline reference
1.0*MEB 100%	60.2 (4.15)	490	Dome Apex	1.16E+06	156	10,480	67[a]	Conservative-estimate gas composition w/100% riser
MAB CE9800 100%	57.7 (3.98)	380	Dome Apex	1.10E+06	139	9800	58	Conservative-estimate gas composition w/100% riser
MAB CE9300 100%	56.8 (3.92)	340	Dome Apex	1.06E+06	150	9300	53	Conservative-estimate gas composition w/100% riser
MAB CE9300 100%	56.4 (3.89)	340	Dome Apex	1.06E+06	150	9300	53	Conservative-estimate gas composition w/100% MPR
MAB CE9300 0%	59.7 (4.12)	340	Dome Apex	No data	No data	9300	No data	Conservative-estimate gas composition w/0% MPR
MAB CE9000 0%	59.0 (4.07)	320	Dome Apex	No data	No data	9000	60	Conservative-estimate gas composition w/0% MPR
MAB CE8654 0%	57.3 (3.95)	295	Dome Apex	1.06E+06	134	8654	49	Conservative-estimate gas composition w/0% MPR
MAB CE8654 66%	55.1 (3.80)	295	Dome Apex	1.01E+06	179	8654	48	Conservative-estimate gas composition w/66% MPR
MAB CE7750 66%	51.3 (3.54)	250	Dome Apex	9.09E+05	179	7750	No data	Conservative-estimate gas composition w/66% MPR
MAB CE6840 100%	47.1 (3.25)	170	Dome Apex	7.86E+05	150	6840	No data	Conservative-estimate gas composition w/100% riser

[a]The velocity of 67 in./s is not the maximum because the program was aborted before completion.

TABLE 5 (CONT)
PARAMETERS OF BURN PRESSURE TRANSIENTS

Burn Case	Peak Pressure (psia) (bar)	Rate of Pressure dP/dt (psia/s)	Spark Location	Total Combustion Energy (Btu)	Average Flame Velocity (ft/s)	Total Gas Release Volume (ft³)	Max. Dome Velocity (in./s)	Remarks
0.65 MEB	47.0 (3.25)	490	Dome Apex	7.61E+05	154	6840	37	Artificially high rate of pressure rise
1.0 MEB Best Estimate	54.0 (3.725)	300	Dome Apex	9.86E+05	134	10,480	45	Best-estimate composition w/100% riser
1.0MEB Best Estimate	56.9 (3.93)	300	Dome Apex	1.06E+06	129	10,480	54	Best-estimate composition w/0% riser

The above variables have been parameterized to understand the relationships better between peak pressures and GRE volumes, pressurization rates, and GRE volumes, and also between peak pressure and pressurization rates. These relationships will aid in determining values of peak pressures and pressurization rates for a given GRE volume without the necessity of performing additional HMS/TRAC burn calculations. It should be understood that these relationships are valid only for a dome apex (top-down) burn spark ignition source and for ranges of GRE volumes between 6500 and 10,500 ft³.

Peak Pressure vs Gas Release Volume
Conservative Estimate Gas Composition

$Y = M0 + M1*x + ... M4*x^4$	
M0	1199.9
M1	-0.56934
M2	0.0001033
M3	-8.1744e-09
M4	2.3963e-13
R	0.99997

4th Order Polynomial

HMS Data - Top Burn

Pressure (psia)

Gas Release Volume (ft^3)

Fig. 23. Peak pressure vs gas release volume.

Peak Pressure vs Pressurization Rate (dP/dt)
Conservative Estimate Gas Composition

$Y = M0 + M1*x + ... M3*x^3$	
M0	36.065
M1	0.05886
M2	5.8883e-05
M3	-1.6064e-07
R	0.99504

3rd Order Polynomial

HMS Data - Top Burn

Pressure (psia)

Pressurization Rate dP/dt (psia/sec)
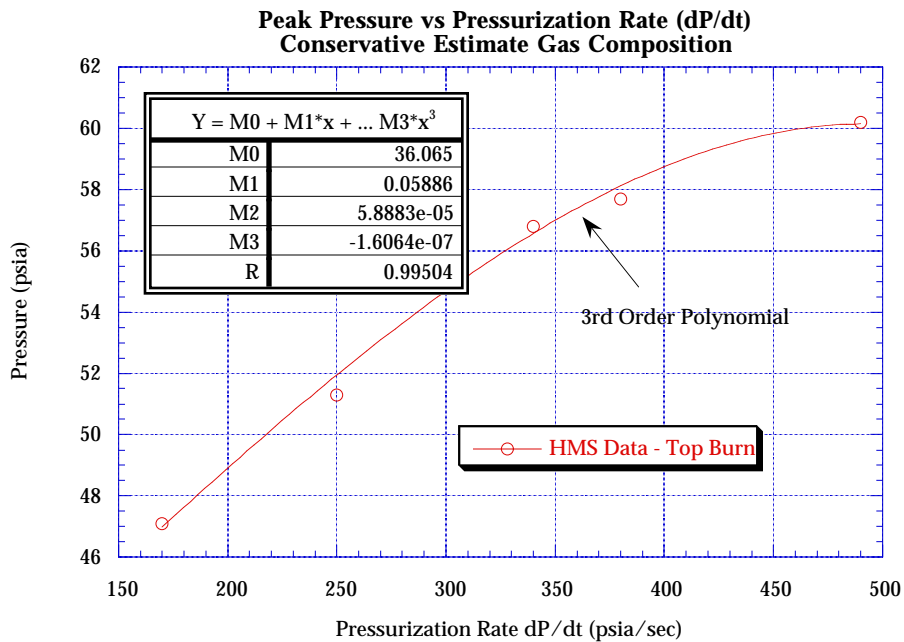
Fig. 24. Peak pressure vs pressurization rate (dP/dt).

33

2.0. MAXIMUM ALLOWABLE BURP (MAB) 9300-ft^3 GRE FOR THE CONSER-VATIVE GAS COMPOSITION WITH AN MPR VENT-FLOW AREA OF 100%

Iterations of gas release volumes were conducted with HMS/TRAC, producing the P-T histories, as noted in Table 5. From the results of the parametric analyses, and recognizing that the 1.0*MEB burn case with a gas volume of 10,480 ft^3 would not satisfy structural limits, the MAB tank structural limit has been determined for a top-down burn spark ignition source.

The structural integrity of Tank 101-SY has been determined for a maximum gas release volume of 9300 ft^3, producing a 3.92-bar (56.8-psia) peak pressure at a pressurization rate of 340 psia/s, with 100% vent flow through the MPR. Additional response parameters are shown in Figs. 25 through 28. This burn case resulted in extensive concrete cracking throughout the dome but with acceptable stresses and strains throughout the tank primary liner structure and rebar, which are below values that would account for structural failure.
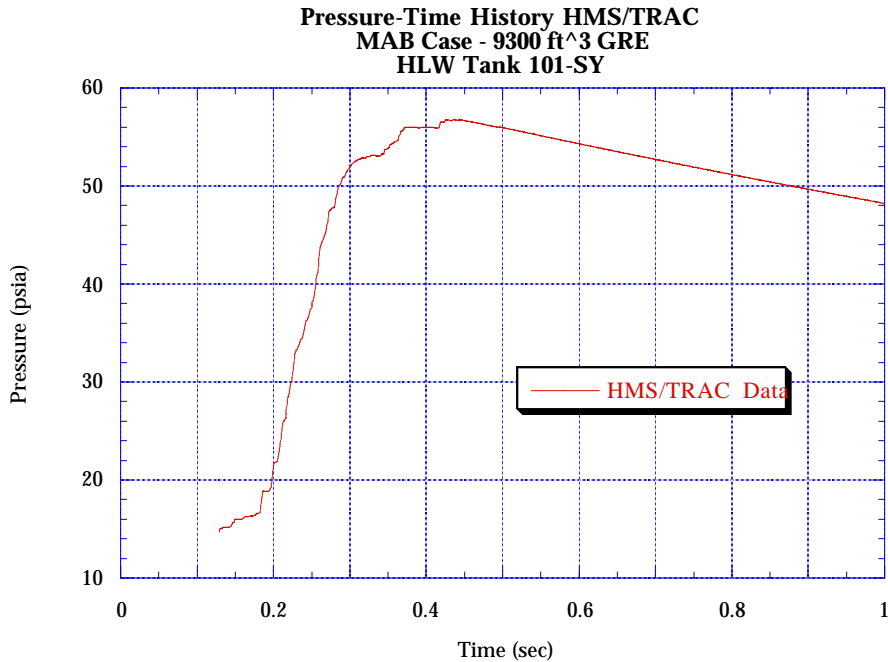
Fig. 25. HMS/TRAC P-T history for a 9300-ft^3 GRE.

Pressure-Time History HMS/TRAC
MAB Case - 9300 ft^3 GRE
HLW Tank 101-SY
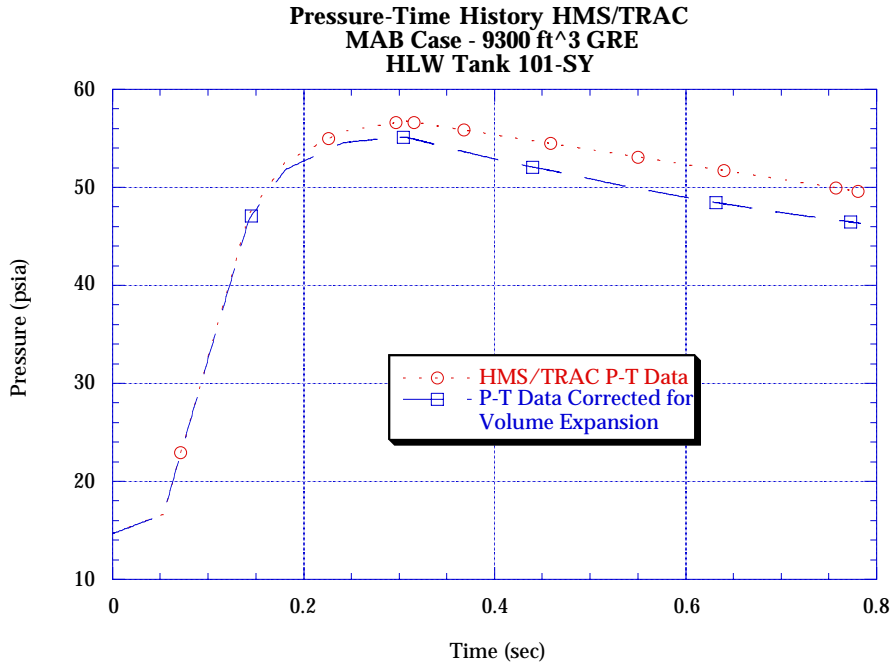
Fig. 26.   Linearized   P-T   history   and   tank   pressure   corrected   for
volumetric expansion.

The maximum dome velocity is shown to be 53 in./s, which is below the threshold
limit to cause failure from reimpaction of the pump pit and soil overburden.

It is evident from Figs. 29 and 30 that a high-frequency resonance in the dome
structure has been excited from ~0.25 to 0.35 s. This can be attributed to the radial
reinforcing bars at the apex, where the concrete has cracked completely. Additional
response data are shown in Figs. 31 and 32.

As can be seen, the whole structure displaces uniformly, with a ~3-in. difference
from the tank base to the dome apex. Figure 33 shows the dome apex displacement-
time history. The maximum displacement is ~10.5 in. and peaks ~0.72 s into the
transient. Figure 34 shows the dome displacement of ~8 in. at the MPR (20-ft radius)
location. Figures 35 through 37 show response parameters for other tank locations.

The results of this analysis show the structural adequacy and integrity of
Tank 101-SY to the 9300-ft^3 burn pressure transient.

Velocity-Time History Selected Locations
MAB Case - 9300 ft^3 GRE
HLW Tank 101-SY

Fig. 27. Velocity-time history for selected locations.
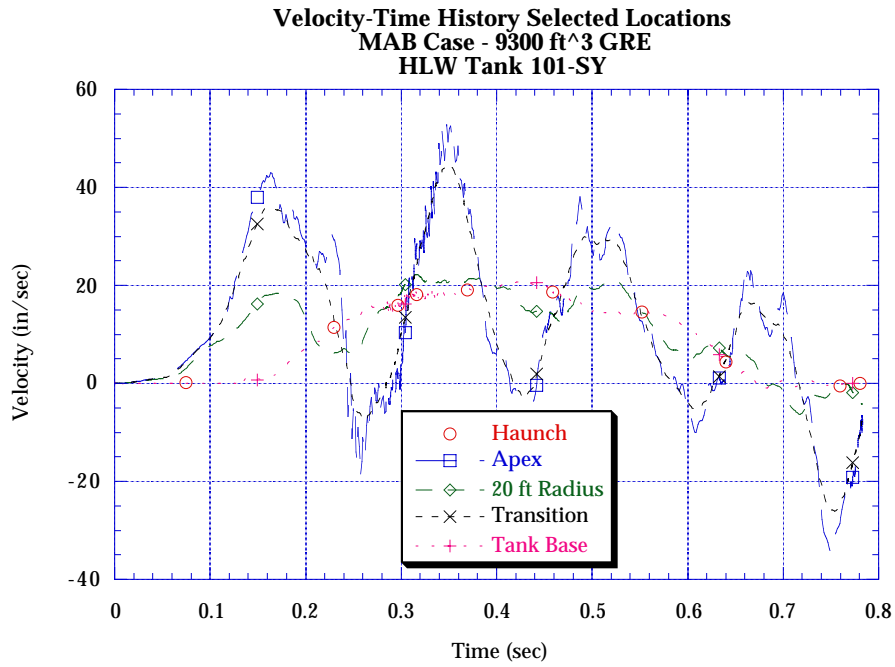
Velocity-Time History Apex
MAB Case - 9300 ft^3 GRE
HLW Tank 101-SY
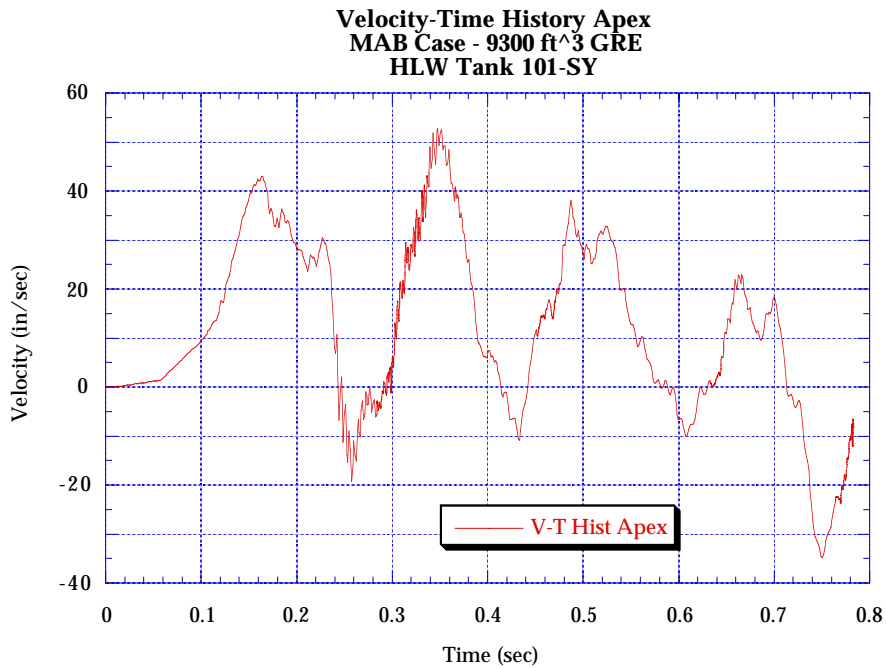
Fig. 28. Dome apex velocity trace (0 to 0.8 s).

36

Velocity-Time History Apex
MAB Case - 9300 ft^3 GRE
HLW Tank 101-SY
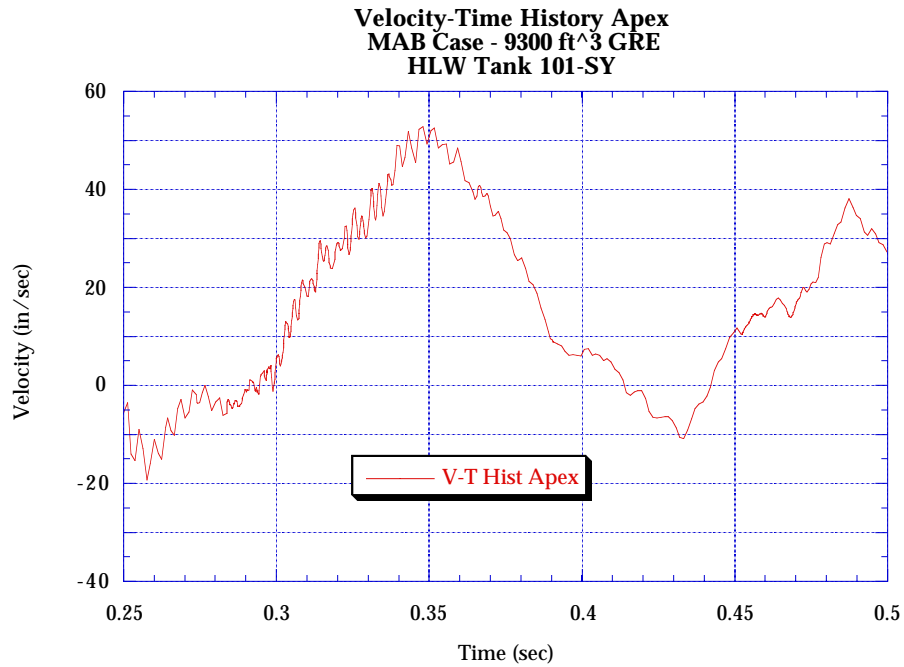
Fig. 29. Dome apex velocity trace, where a high-frequency resonance in the dome structure has been excited from ~0.25 to 0.35 s.

Velocity-Time History Apex
MAB Case - 9300 ft^3 GRE
HLW Tank 101-SY
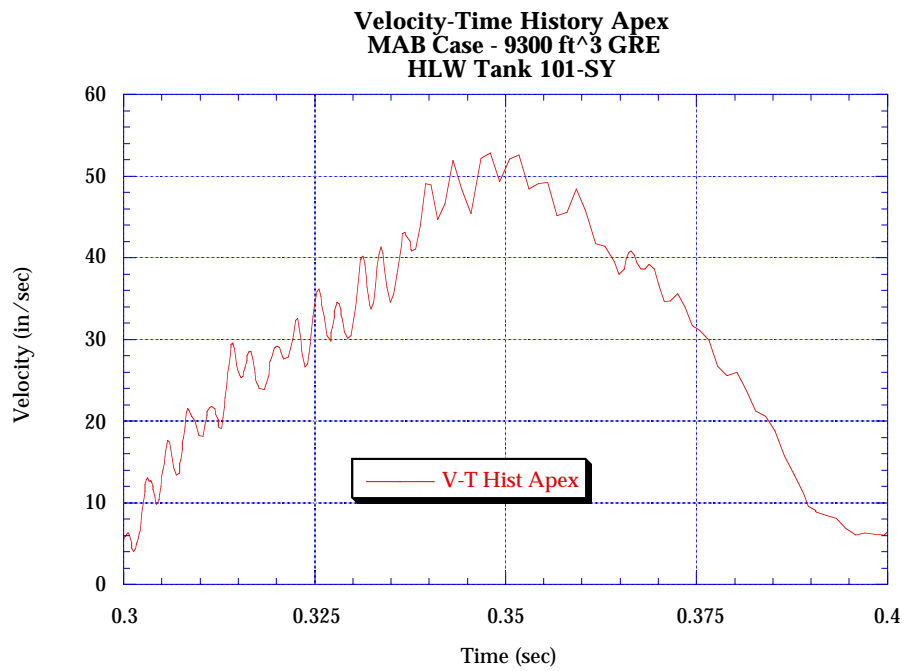
Fig. 30. Dome apex velocity trace (0.3 to 0.4 s).
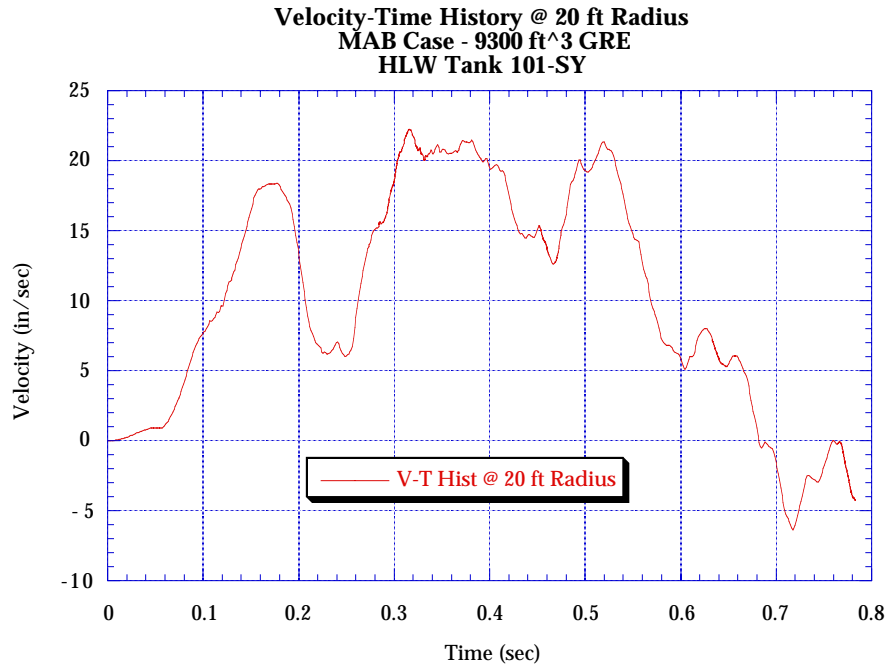
Fig. 31. Velocity-time history at the dome's 20-ft radius location.
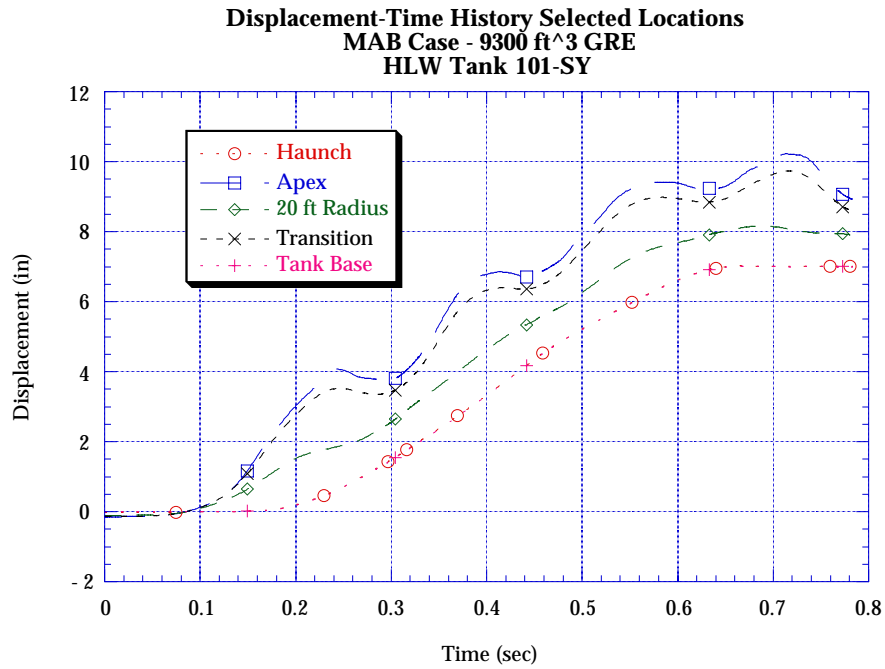
Fig. 32. Displacement histories for selected locations on the tank structure.
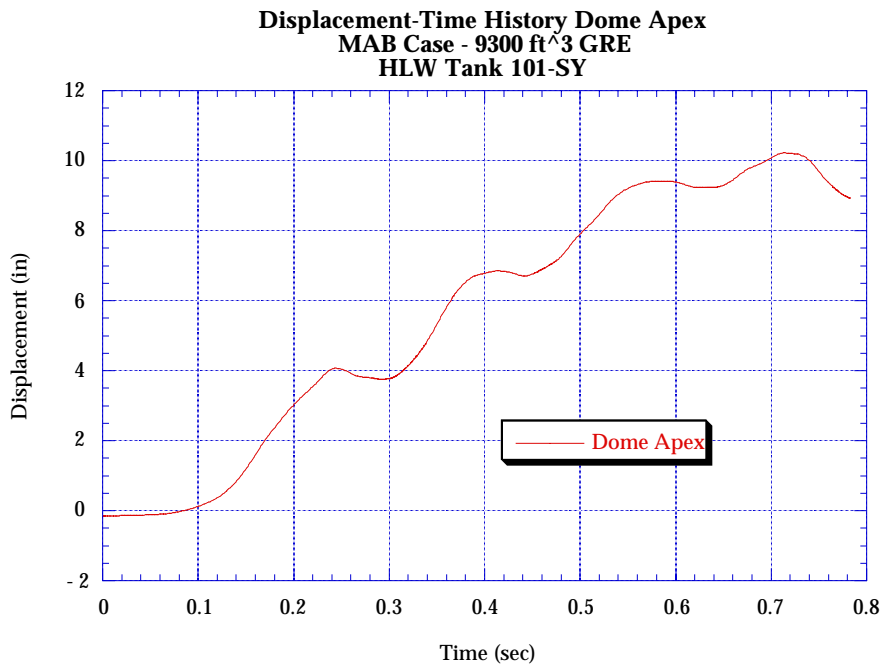
Fig. 33. Dome apex displacement-time history.
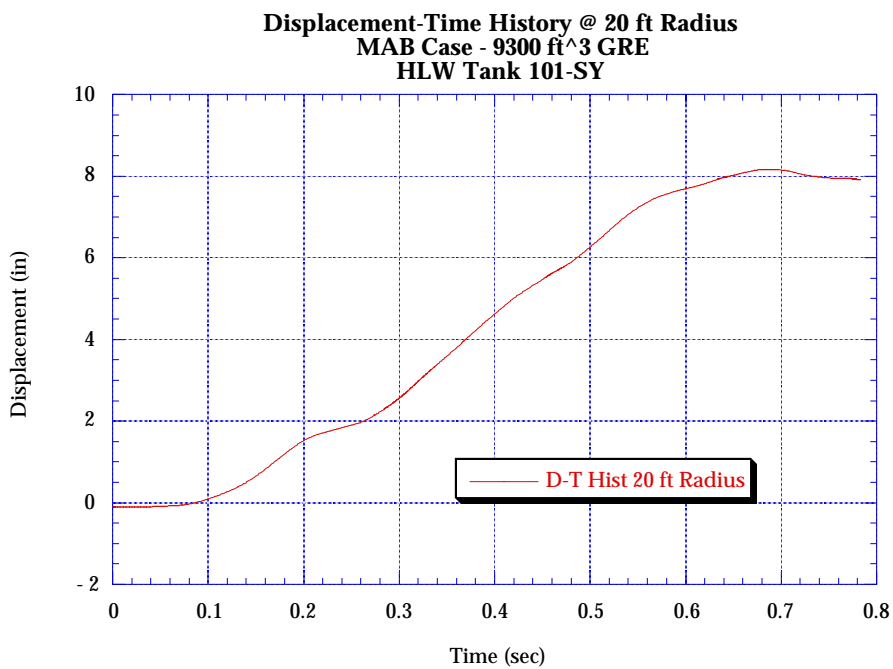
Fig. 34. Dome displacement of ~8 in. at the MPR (20-ft radius) location.
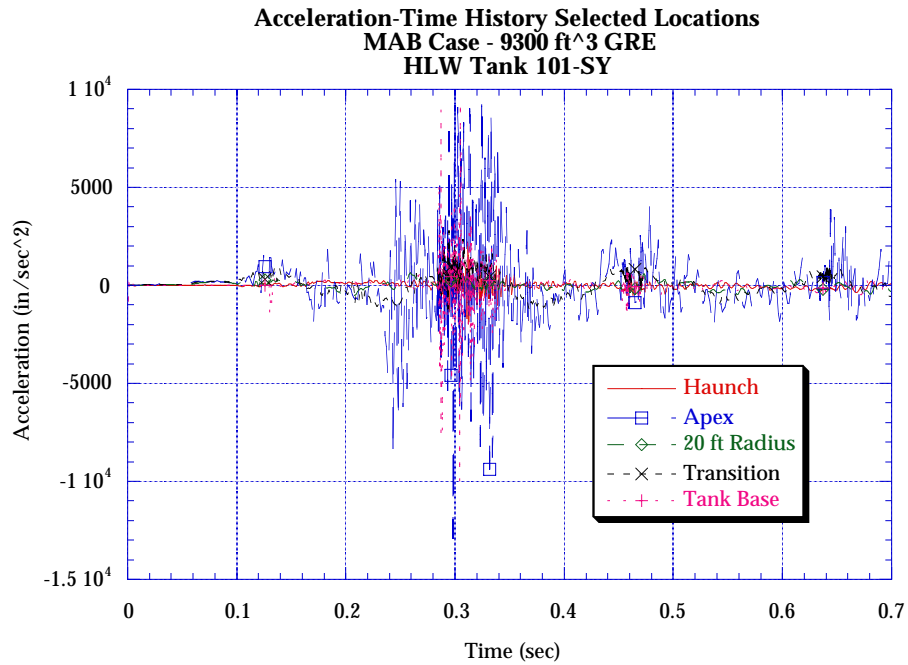
Fig. 35. Acceleration-time history for selected locations on the tank structure.
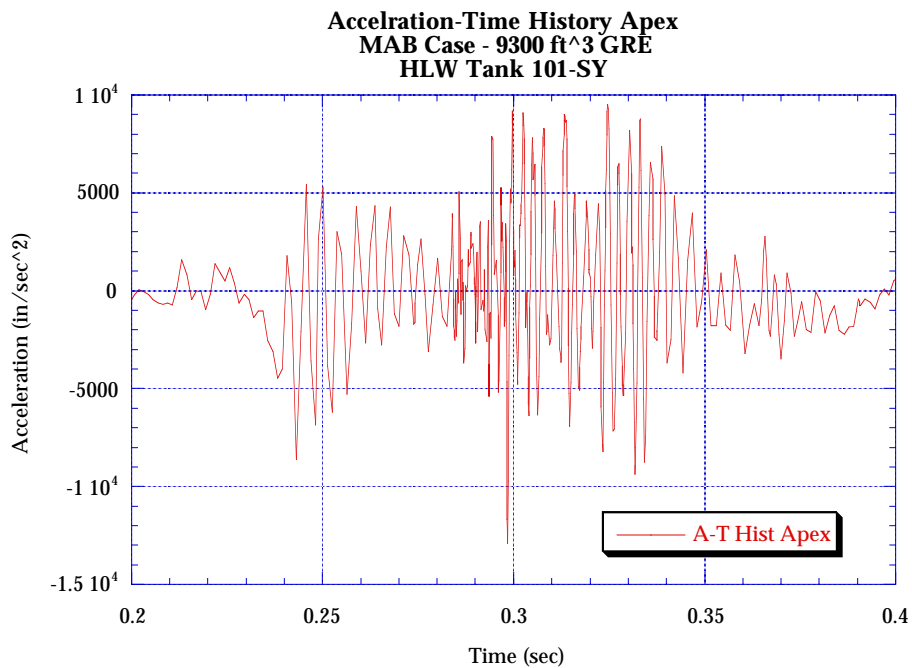
Fig. 36.   Acceleration-time histories for the dome apex and the MPR location at the 20-ft radius (0.2 to 0.4 s).

Acceleration-Time History @ 20 ft Radius
MAB Case - 9300 ft^3 GRE
HLW Tank 101-SY
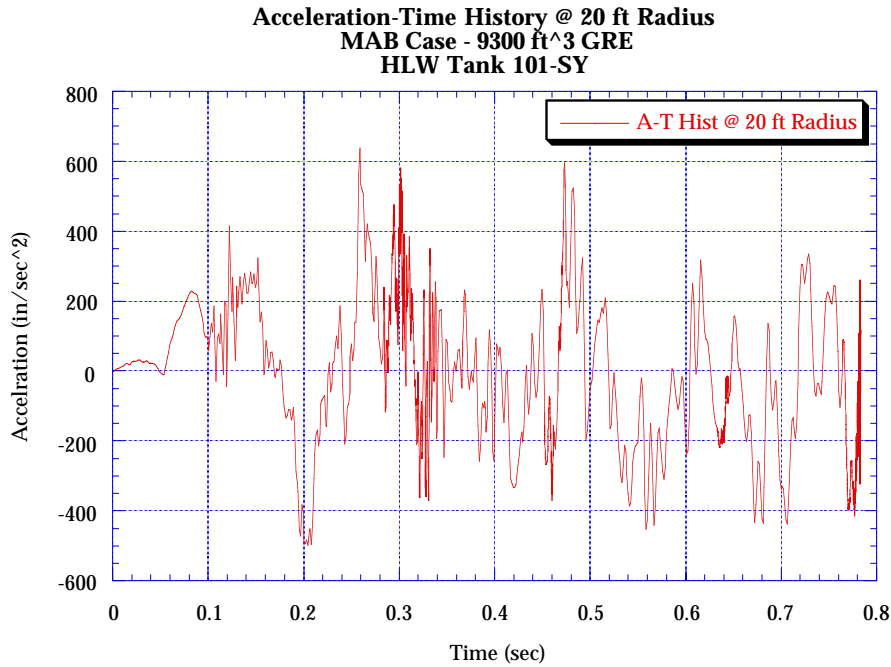
Fig. 37.   Acceleration-time   histories   for   the   MPR   location   at   the 20-ft radius (0 to 0.8 s).

3.0.   MAXIMUM ALLOWABLE BURP (MAB) OF 9800-ft^3 GRE FOR A CONSER-VATIVE GAS COMPOSITION WITH AN MPR VENT FLOW AREA OF 100%

To determine whether the 9300-ft^3 GRE was in fact the limiting gas volume, a structural analysis for a slightly higher volume at 9800 ft^3 was performed. The analysis was completed successfully without any numerical difficulties. This GRE exhibited a peak pressure of 3.98 bar (57.7 psia) at a pressurization rate of 380 psia/s, as shown in Figs. 38 and 39. However, the peak dome velocity exceeded the threshold limit of 54.5 in./s to preclude collapse from reimpaction of the pump pit and soil overburden. Figures 40 and 41 show the velocity peak occurring ~0.355 s into the transient. As such, this analysis documents that gas release volumes >9300 ft^3 with 100% vent flow through the MPR and having a conservative gas composition and spark ignition source at the dome apex will not satisfy the structural criteria.

As stated previously, this burn case exceeded the structural capacity of the dome structure to preclude collapse from soil and pump pit reimpaction. Therefore, the MAB structural limit, based on a conservative estimate of gas composition, stands at 9300 ft^3 with a peak pressure of 3.92 bar (56.8 psia).

41
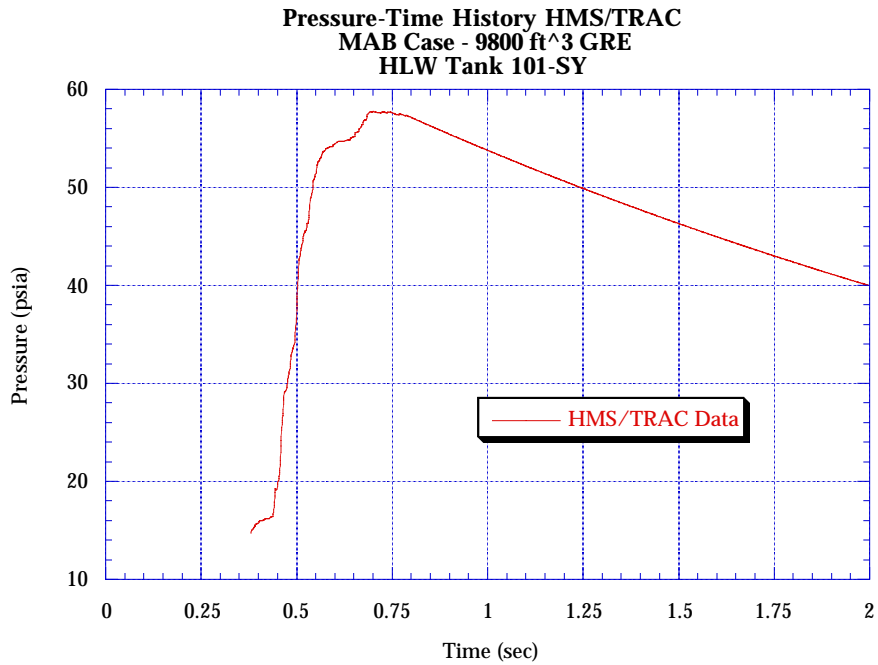
Fig. 38. HMS/TRAC derived P-T history.
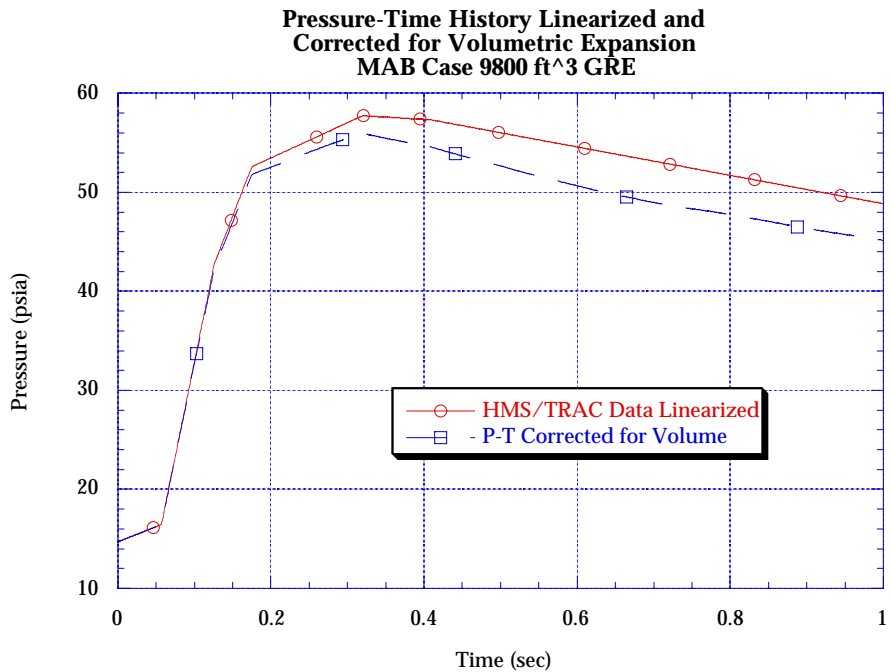
Fig. 39. HMS/TRAC linearized P-T history, as well as history corrected for volumetric expansion (0 to 1 s).

Velocity-Time History Dome Apex
MAB 9800 ft^3 GRE
HLW Tank 101-SY
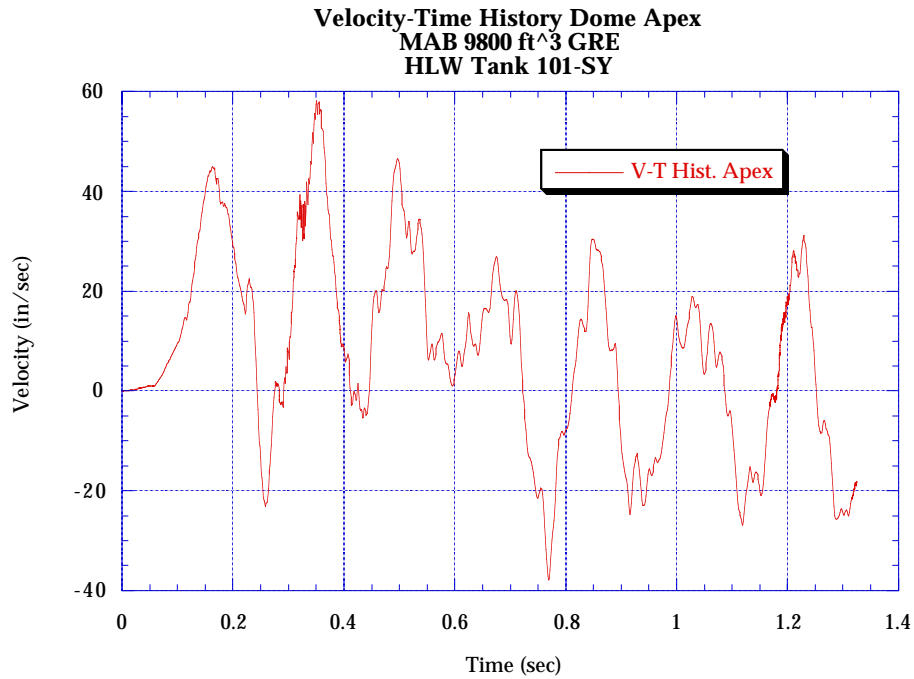
Fig. 40. Velocity-time history of the dome apex.

Velocity-Time History Dome Apex
MAB 9800 ft^3 GRE
HLW Tank 101-SY
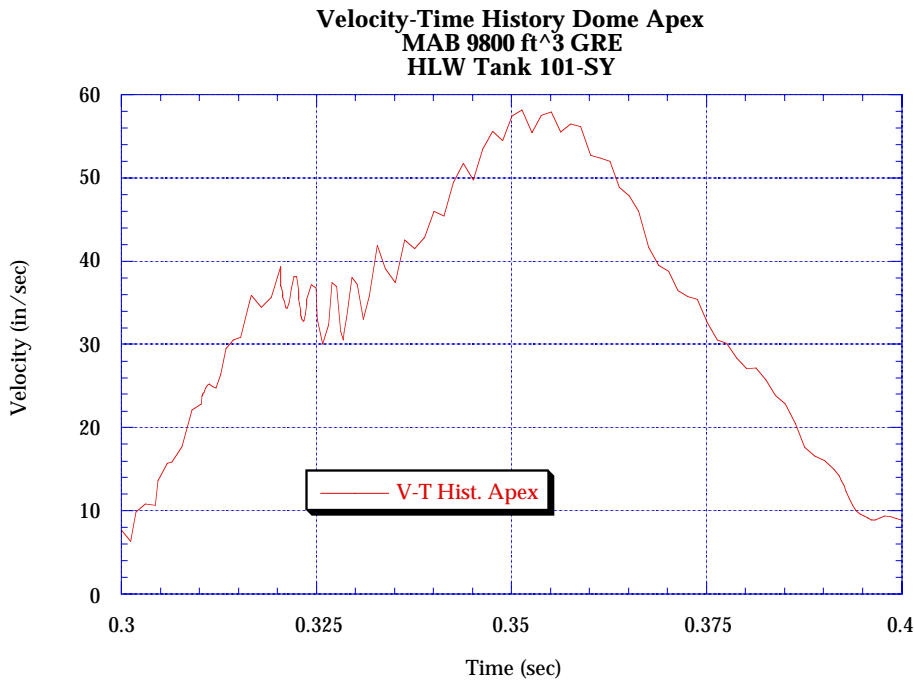
Fig. 41. Peak velocity at the apex from 0.3 to 0.4 s into the transient.

4.0. MAXIMUM ALLOWABLE BURP (MAB) OF 8654-ft^3 GRE FOR A CONSER-VATIVE GAS COMPOSITION WITH AN MPR VENT-FLOW AREA OF 0%

Because a 9300-ft^3 GRE with 0% vent flow through the MPR did not satisfy the structural criteria, it was necessary to determine the gas volume that would provide structural integrity of Tank 101-SY. The burn scenario was obtained for the 8654-ft^3 GRE (which was the maximum window burp) at 0% vent flow. Figure 42 shows the P-T history for the 0% vent-flow case of the 8654-ft^3 GRE. The linearized P-T histories and the P-T histories corrected for volumetric expansion of the tank are shown in Fig. 43.

The 0% riser area case exhibited a peak pressure at 3.95 bar (57.3 psia), with a pressurization rate of 295 psia/s. As expected, the P-T history depicts no depressurization characteristic, as shown in Fig. 42.

Although the solution completed without any numerical difficulties, a characteristic resonance was evident at the dome apex, as shown in Figs. 44 through 46. This resonance was attributed previously to a fundamental frequency in the dome being excited at the driving frequency of the pressure pulse. However, unlike previous analyses where the solution aborted because of amplifications in the range of 1.5 to 1.8, this solution progressed smoothly.

The peak velocity at the apex is ~50 in./s, which is below the threshold value of 54.5 in./s to preclude dome failure from reimpaction of the soil overburden and the pump pit. As previously mentioned, a slight chattering, or high-frequency response, occurred in the dome apex ~0.3 to 0.4 s into the transient. The high-frequency chatter shown in Fig. 46 dampened without numerical failure of the program. Other response parameters are shown in Figs. 47 through 53.
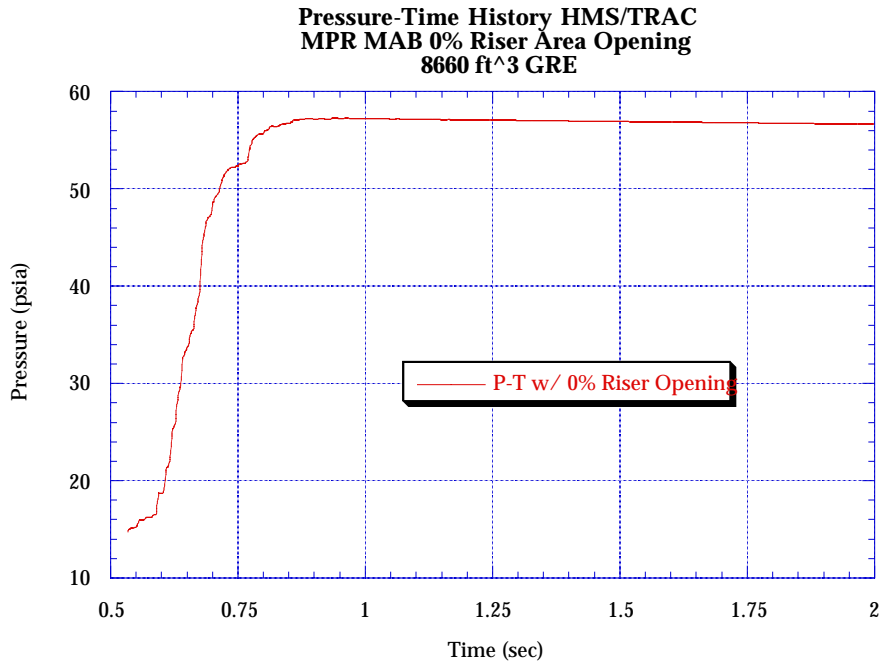
Fig. 42. P-T history for 0% riser opening.
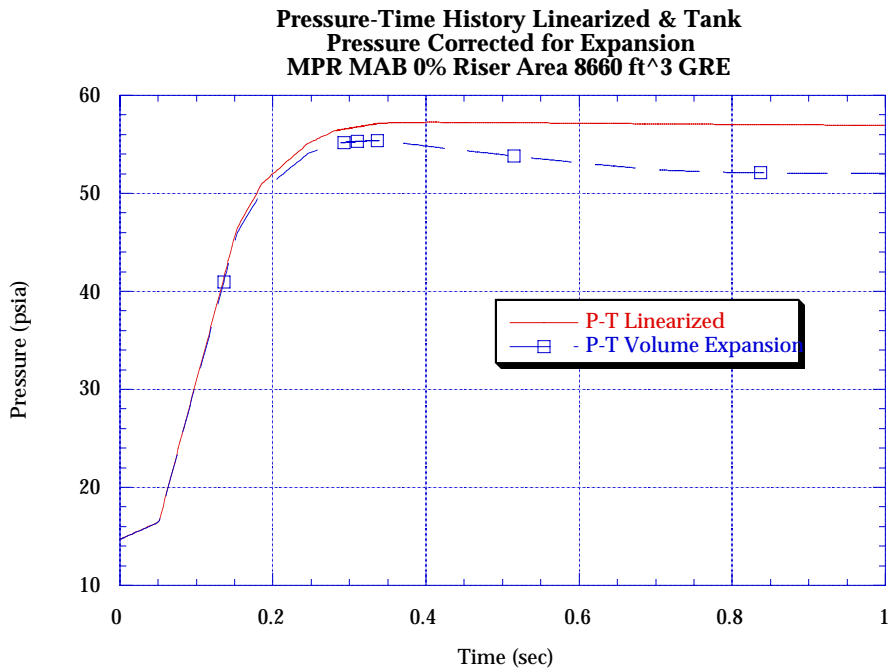
Fig. 43. Linearized P-T history and correction for expansion.
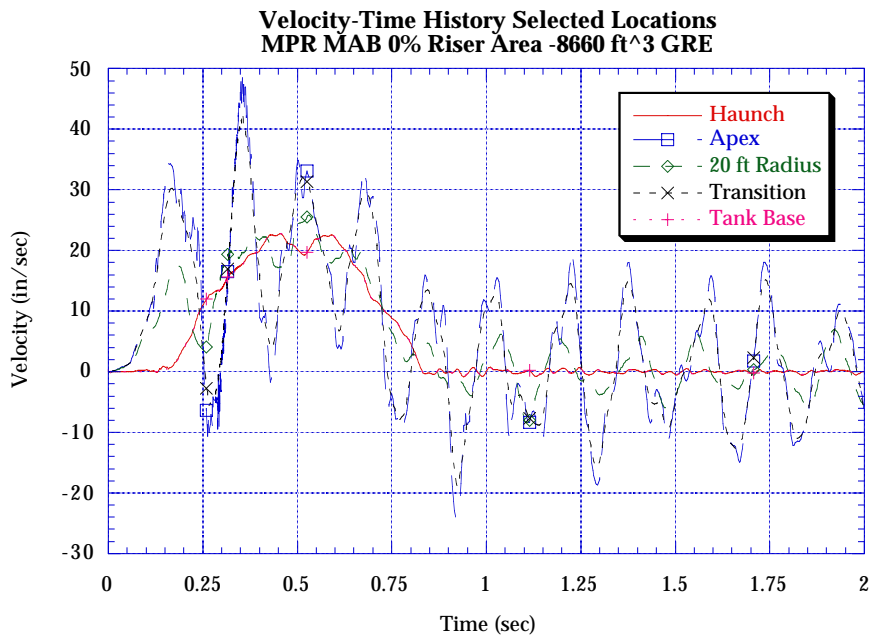
Fig. 44. Velocity-time history for selected locations with a 0% riser area.
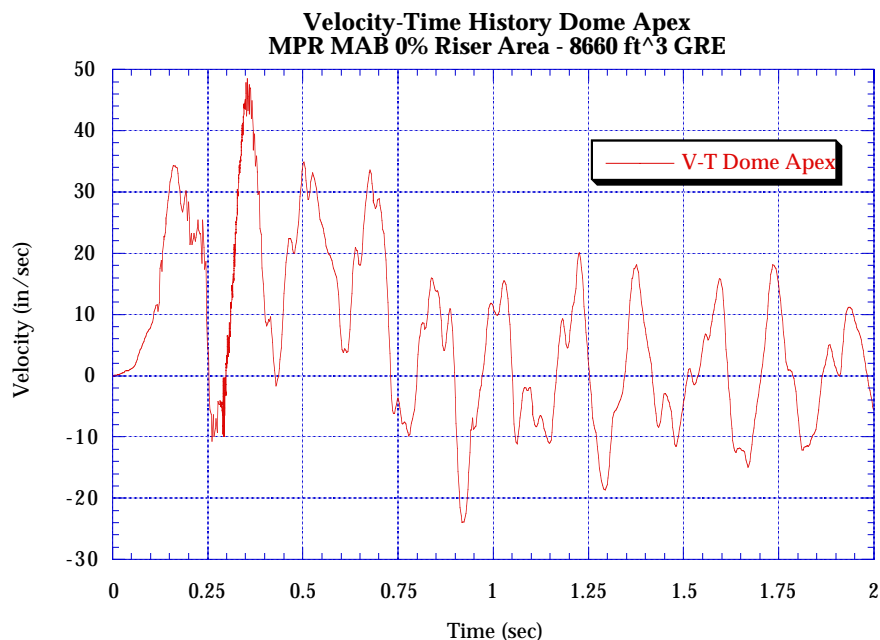
Fig. 45. Velocity-time history dome apex with a 0% riser area.
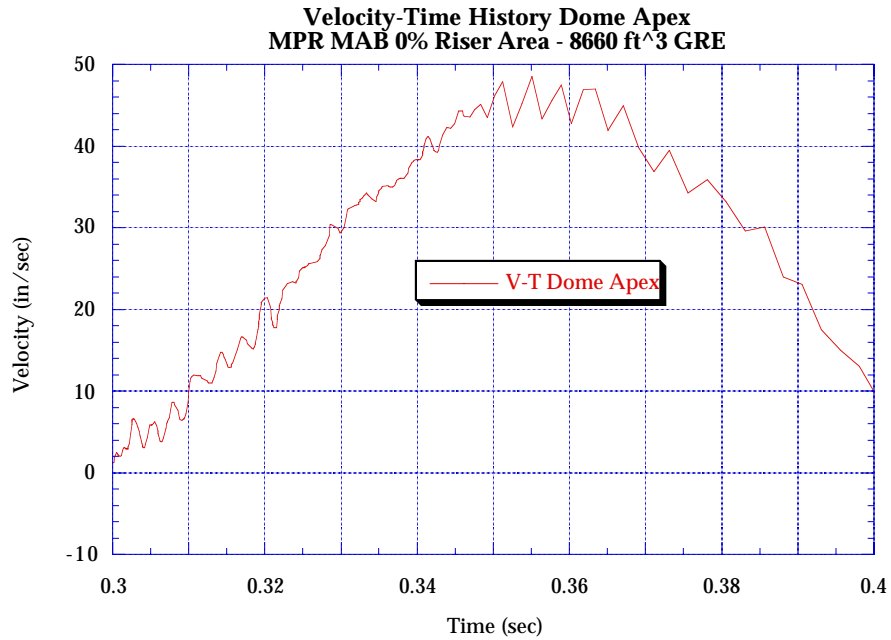
Fig. 46. Velocity-time history dome apex with a 0% riser area.
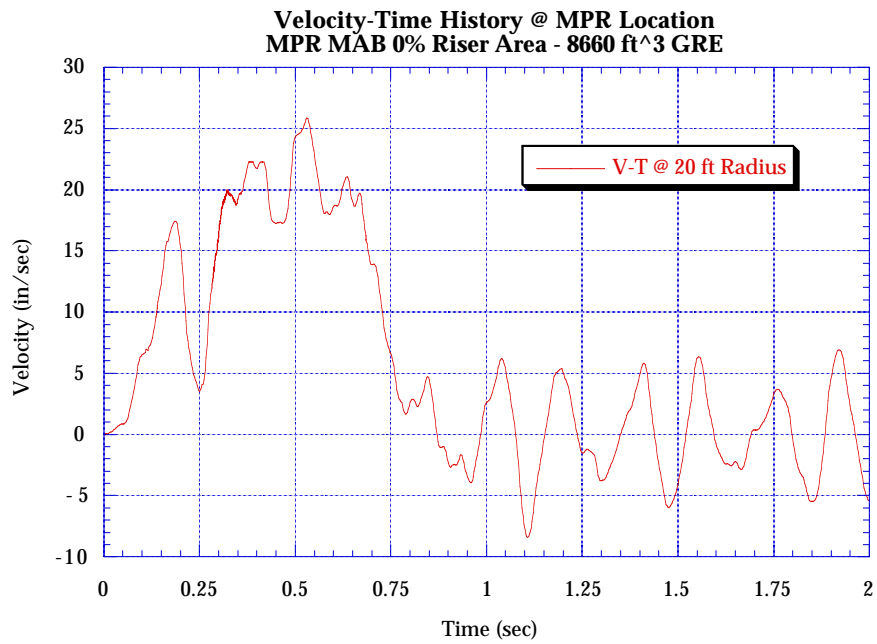
Fig. 47. Velocity-time history MPR location with a 0% riser area.
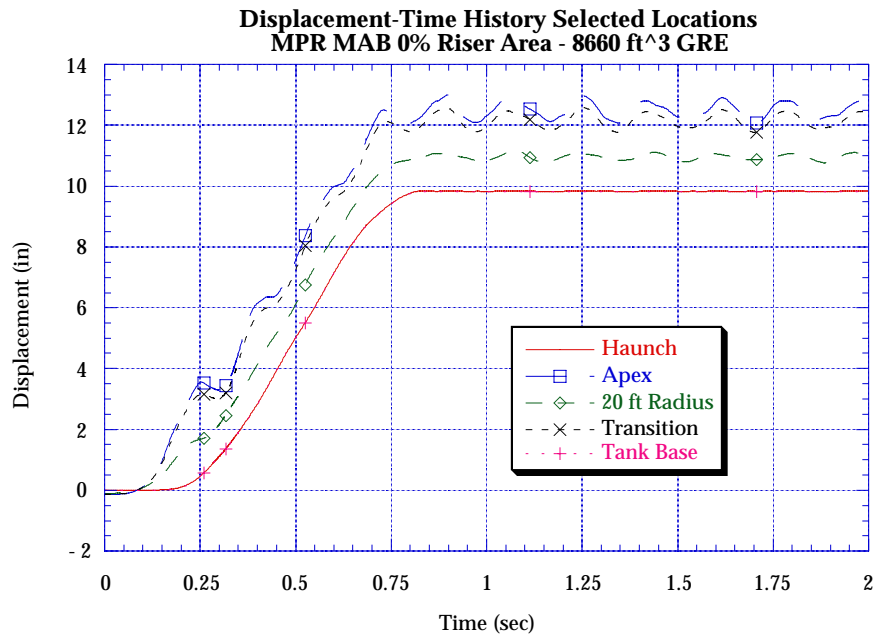
Fig. 48. Displacement-time history for selected locations with a 0% riser area.
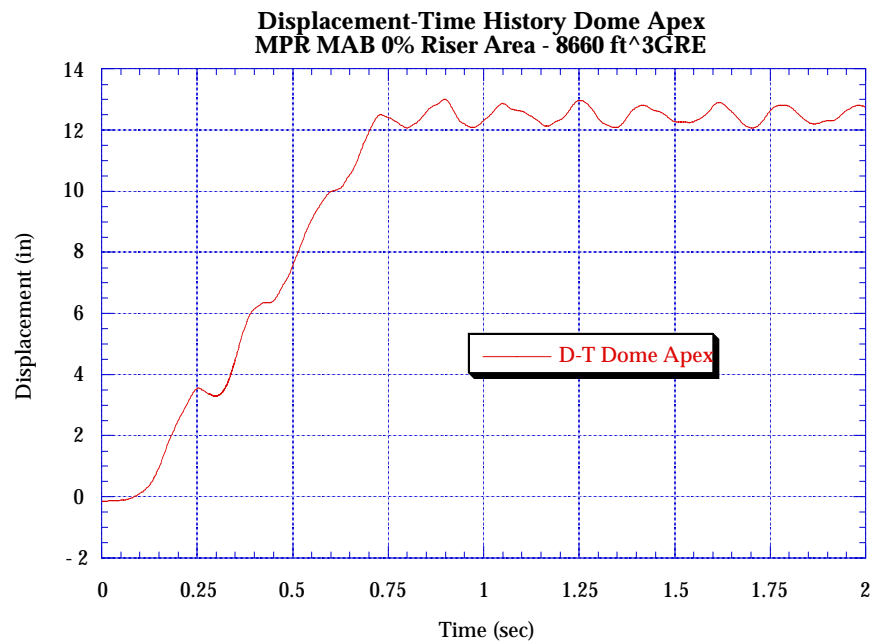
Fig. 49. Displacement-time history for dome apex with a 0% riser area.
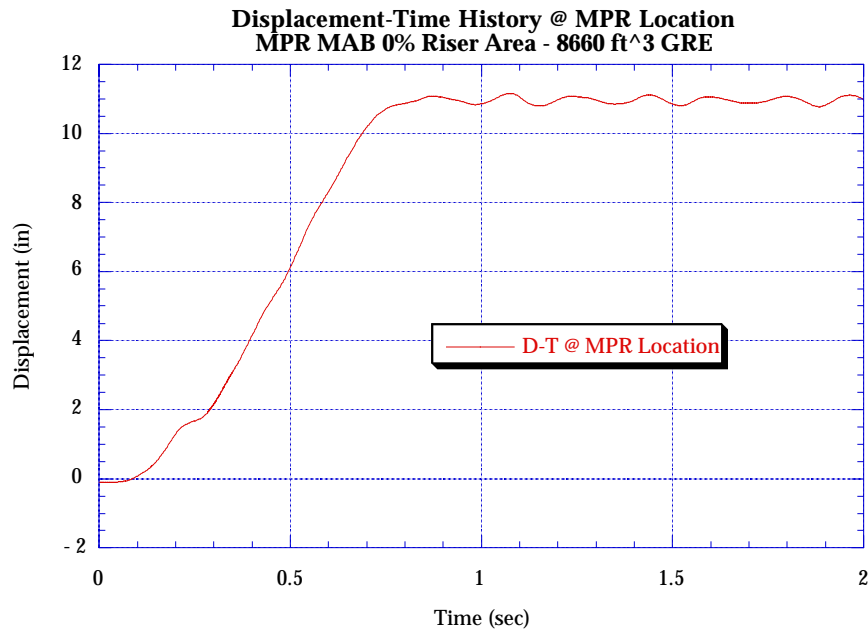
Fig. 50. Displacement-time history for MPR location with a 0% riser area.
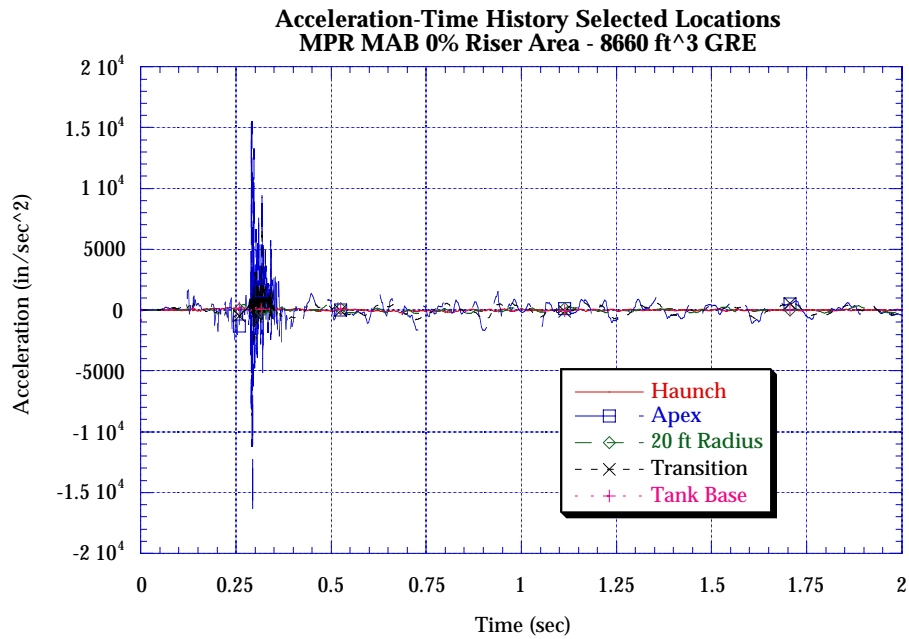
Fig. 51. Acceleration-time history for a selected location with a 0% riser area.

49
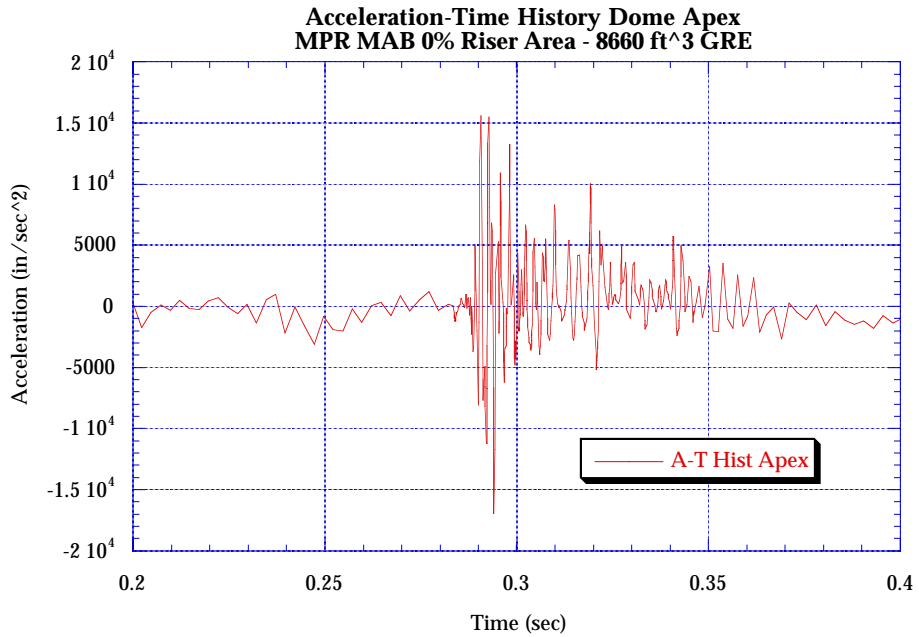
Fig. 52. Acceleration-time history for a dome apex with a 0% riser area.
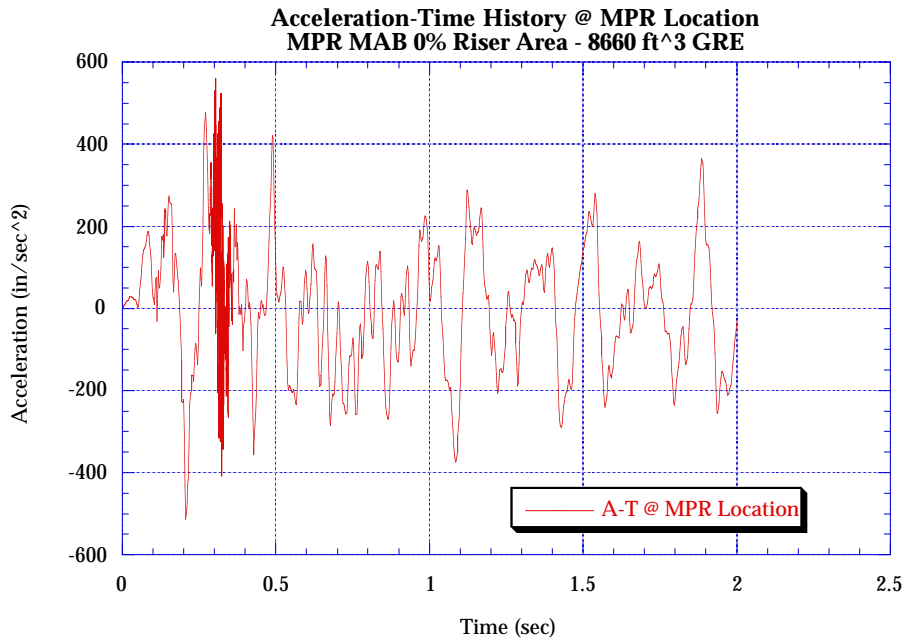
Fig. 53. Acceleration-time history at an MPR location with a 0% riser area.

Rebar yielding was extensive near the dome apex region but nowhere else in the tank. Table 6 shows the strains in the liner and dome rebar.

TABLE 6
TOTAL PLASTIC STRAINS AT SELECTED LOCATIONS

Item	Strain (%)	Limit (%)	Location
Dome Liner	0.85	1.0	Dome Transition
Primary Liner		6.0	Lower Knuckle
Dome Rebars	0.55	6.0	Dome Apex

5.0. SUMMARY FOR APPENDIX B

Appendix B entailed evaluating the MAB burn scenario for a "conservative estimate" of gas composition and gas release rates.

The MAB is set at a 9300-ft^3 GRE with 100% vent-flow area through the MPR. Because the structural analysis for the 9300-ft^3 GRE with 0% vent flow had numerical difficulties, it was necessary to reduce the GRE volume and obtain an adequate structural solution for a lower GRE volume. The 8654-ft^3 GRE burn case with 0% vent flow satisfied the structural criteria.

Dome liner tearing is not expected in either of these cases because the maximum primary liner and rebar strains encountered are bounded by the 1.25*MEB transient, and maximum dome apex velocities are below the critical threshold value to preclude dome collapse.

APPENDIX C

MAB FOR A BEST-ESTIMATE MEB BURN CASE
WITH A DOME SPARK SOURCE LOCATION

1.0. INTRODUCTION

This section focuses on the structural response of Tank 101-SY to a best-estimate MEB hydrogen burn having a spark source located directly under the dome. The volume of gas release for this event is 10,480 ft^3, which is equivalent in volume to the conservative-estimate 1.0*MEB. The gas composition is slightly different than the original baseline reference case and that of Appendix B. In this section, the burn initiates just under the dome, trapping more fuel rather than forcing unburned gases through the vent. Two cases are evaluated for different MPR vent-flow areas of 100% and 0%.

2.0. BEST-ESTIMATE MEB (10,480-ft^3) BURN CASE FOR AN MPR VENT FLOW
AREA OF 100%

Figures 54 and 55 show the P-T history for the best-estimate burn case. This transient produces a peak pressure of 3.725 bar (54.0 psia) at a pressurization rate of 300 psia/s. In comparison, the rate of pressurization (i.e., the linear portion of the curve) is ~300 psia/s vs 490 psia/s for the conservative gas estimate 1.0*MEB case in Fig. 18. Qualitatively, this shows a marked difference in the initial pressure rise of the system, which ultimately has a significant effect on the response of the tank and dome.

Results of the structural analysis show that peak dome velocities are lower than the conservative-estimate 1.0*MEB case, which is expected because of the lower peak pressure. These velocities are well below the threshold for ejecting soil that would cause a reimpaction concern.

The average velocity across the dome at the instant in time where the dome apex exhibits its peak velocity is ~30 in./s. Overall, this dome velocity is well below the threshold for soil reimpaction after separation. Therefore, no concern for dome failure exists. Other response parameters are shown in Figs. 56 through 66.

Pressure-Time History HMS/TRAC
Best Estimate MEB Burn 10,480 ft^3 GRE
HLW Tank 101-SY
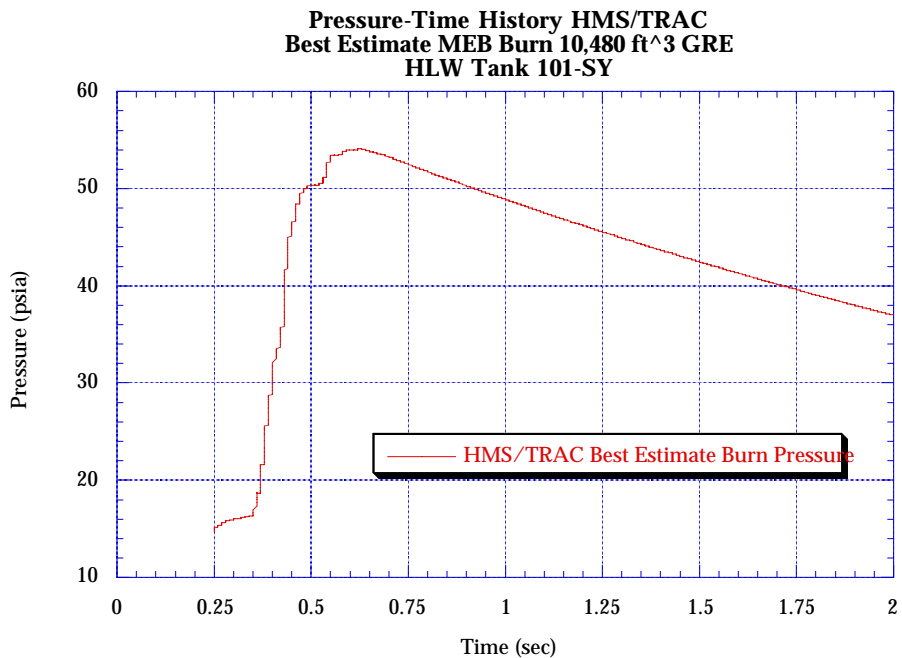
Fig. 54. Best-estimate MEB burn P-T history.

Pressure-Time History & Tank Pressure
Corrected for Volumetric Expansion
Best Estimate MEB Burn 10,480 ft^3 GRE
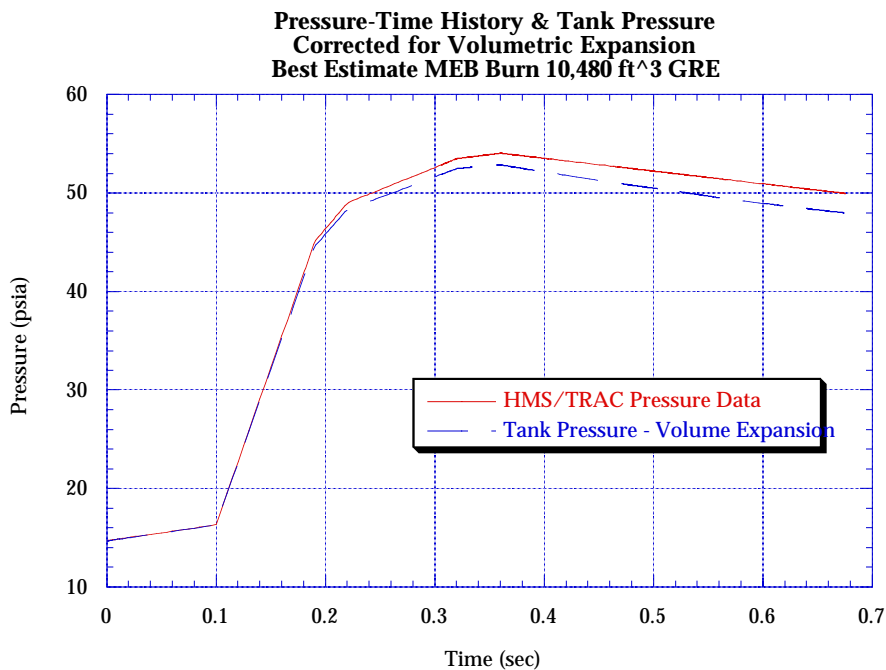
Fig. 55. P-T history corrected for volume expansion.
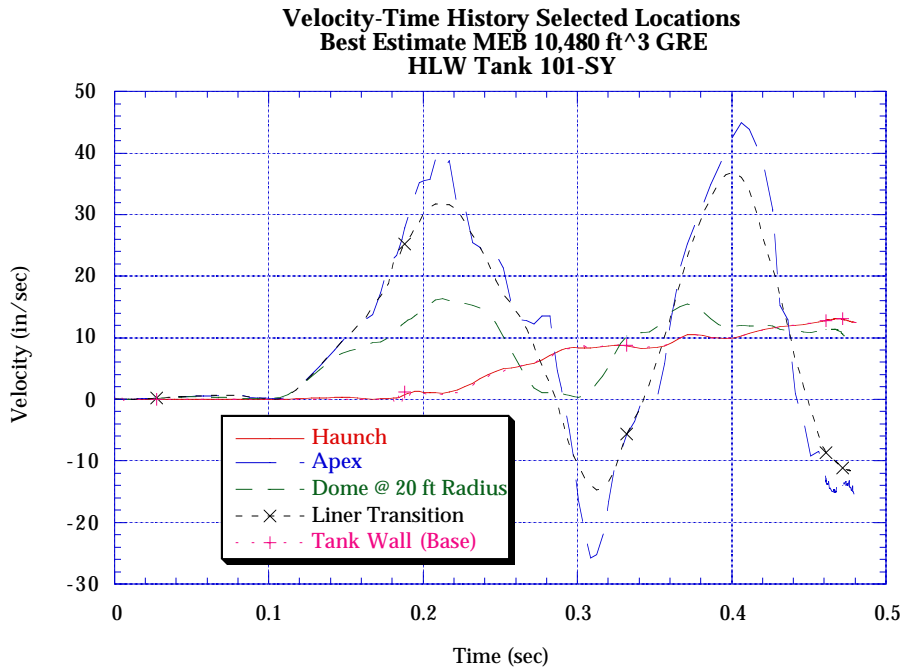
Velocity-Time History Selected Locations
Best Estimate MEB 10,480 ft^3 GRE
HLW Tank 101-SY

Fig. 56. Velocity-time history for selected locations.
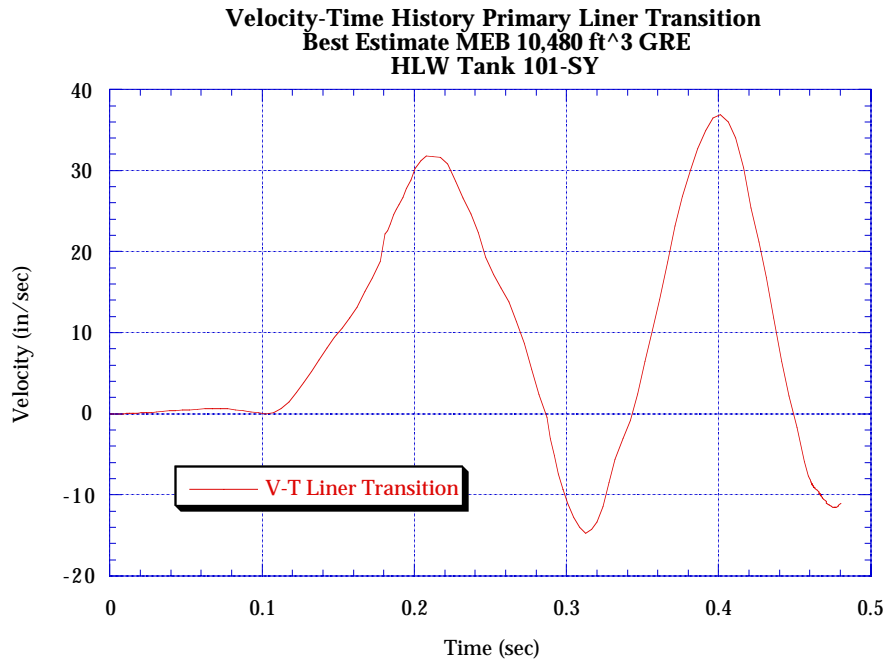
Velocity-Time History Dome Apex
Best Estimate MEB 10,480 ft^3 GRE
HLW Tank 101-SY
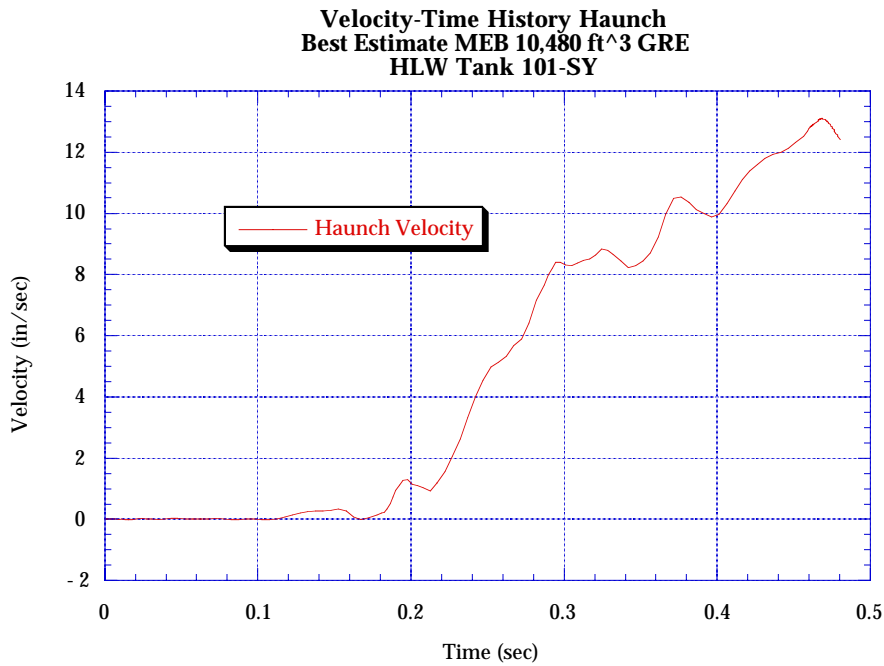
Fig. 57. Dome apex velocity-time history.

In Fig. 64, some high-frequency vibration is exhibited at ~0.45 s. This high frequency is a result of a radial reinforcement bar located directly at the dome apex, where the concrete has cracked completely and therefore has no other stiffness associated with the connection. However, it does not have any detrimental effect anywhere in the dome or tank but shows up as a numerical oscillation.
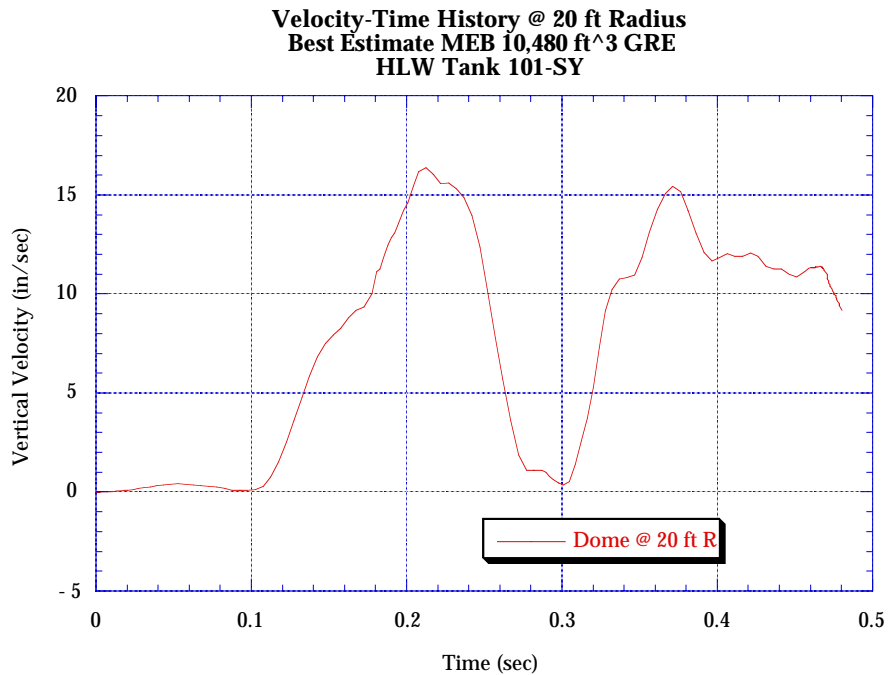
Fig. 60. Velocity-time history of dome at the 20-ft radius location.
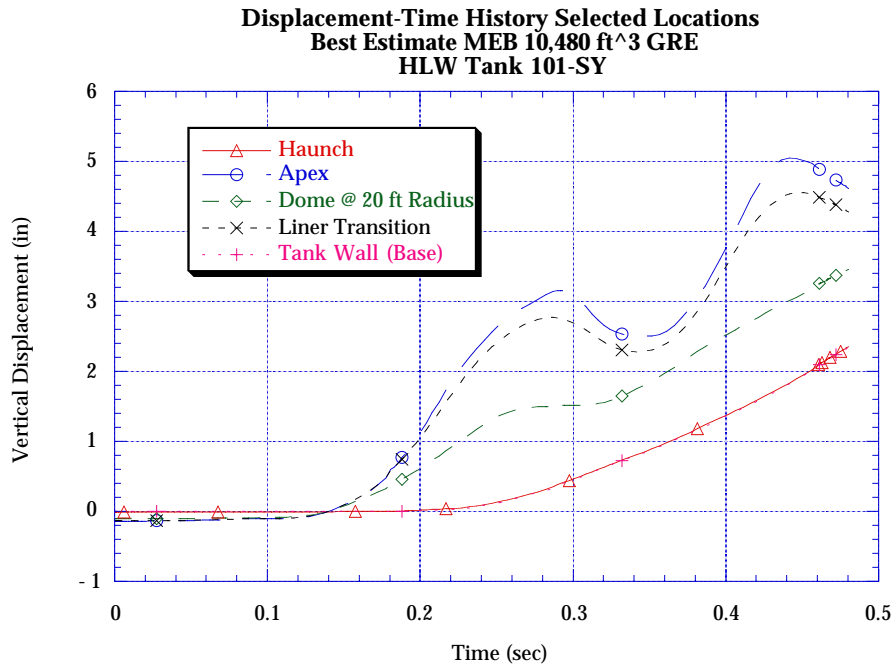
Displacement-Time History Selected Locations
Best Estimate MEB 10,480 ft^3 GRE
HLW Tank 101-SY

Fig. 61. Displacement-time history for selected locations.
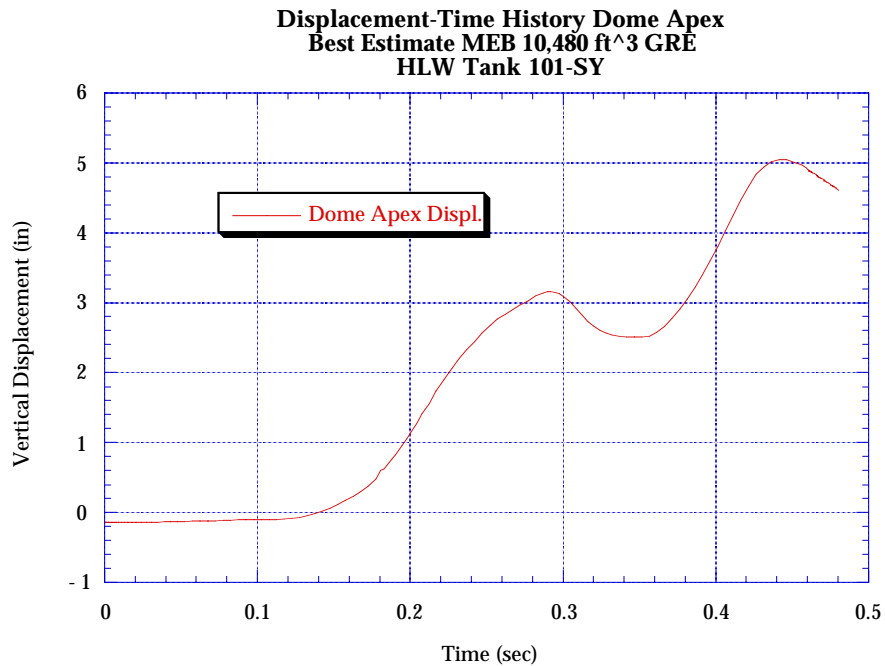
Displacement-Time History Dome Apex
Best Estimate MEB 10,480 ft^3 GRE
HLW Tank 101-SY

Fig. 62. Displacement-time history for dome apex.

Acceleration-Time History Selected Locations
Best Estimate MEB 10,480 ft^3 GRE
HLW Tank 101-SY

Fig. 63. Acceleration-time history for selected locations.

Acceleration-Time History Dome Apex
Best Estimate MEB 10,480 ft^3 GRE
HLW Tank 101-SY
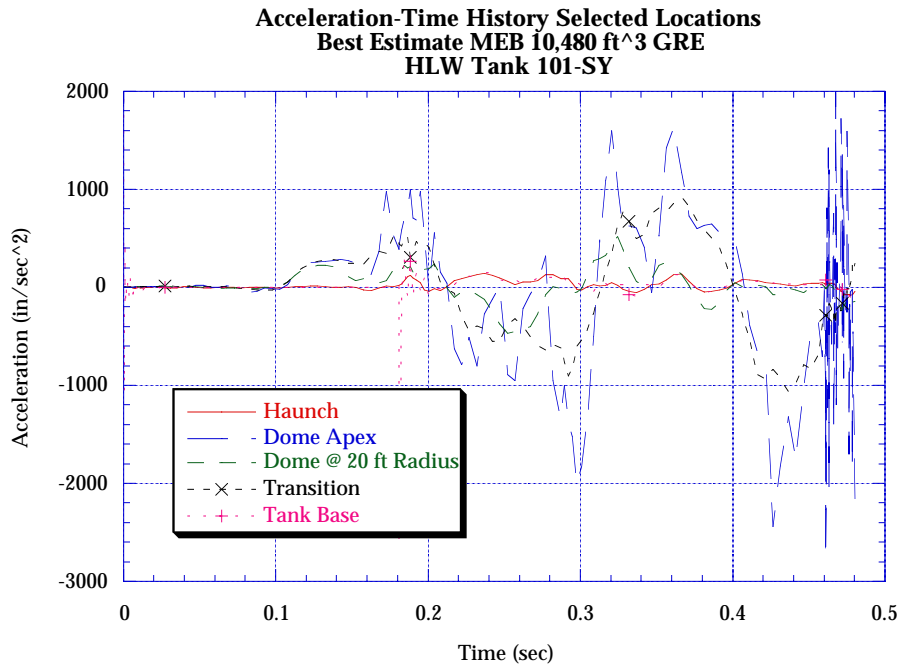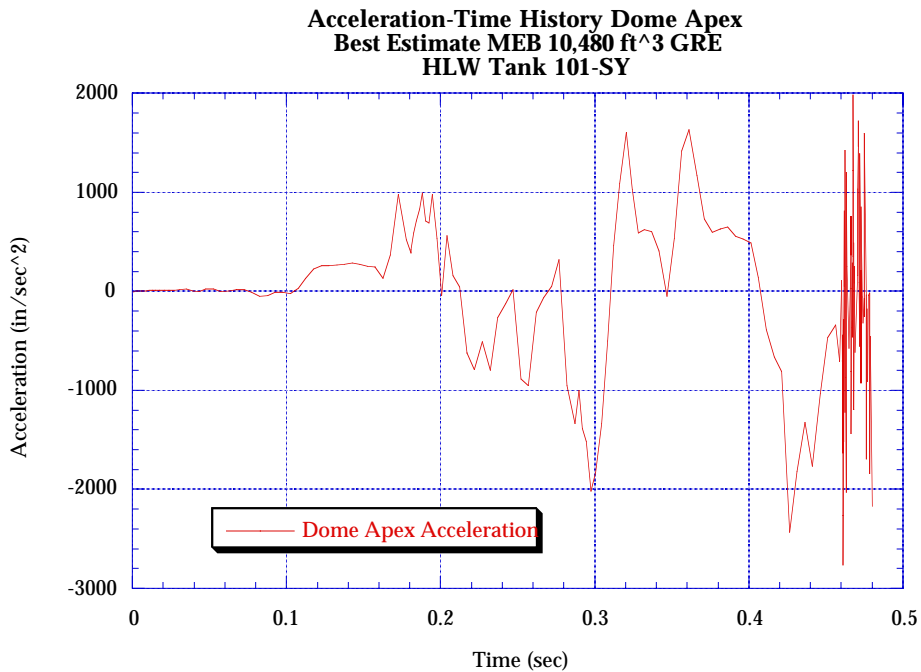
Fig. 64. Acceleration-time history for dome apex.

Acceleration-Time History Liner Transition
Best Estimate MEB 10,480 ft^3 GRE
HLW Tank 101-SY
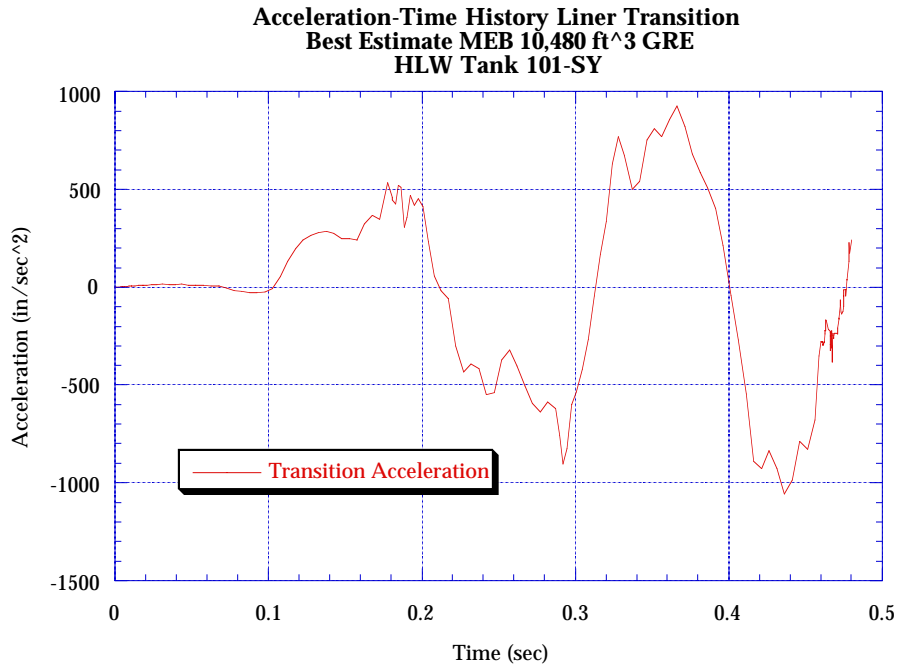
Fig. 65. Acceleration-time history for primary liner transition.

Acceleration-Time History @ 20 ft Radius
Best Estimate MEB 10,480 ft^3 GRE
HLW Tank 101-SY
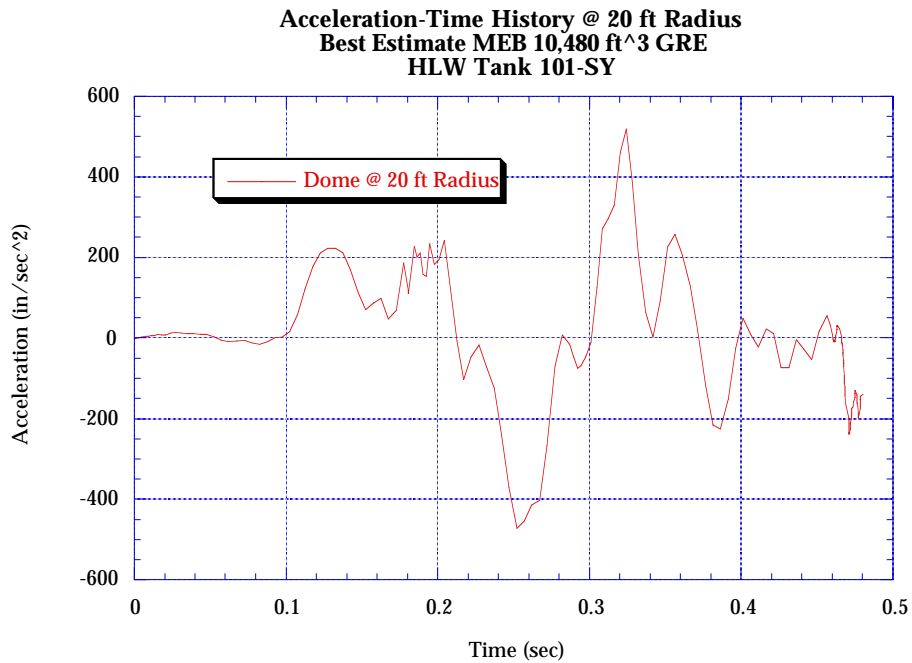
Fig. 66. Acceleration-time history of dome at the 20-ft radius.

Overall stress analysis results show primary liner strains in the vicinity of the thickness transition of ~0.2%, which is well below those found in the original 1.25*MEB baseline reference case. Some concrete cracking was evident throughout the dome, with extensive cracking immediately at the apex. As mentioned previously, the extensive concrete cracking at the apex allowed a radial reinforcing bar to vibrate at high frequency, which was shown on the acceleration-time history of the apex at ~0.45 s. This extensive cracking does not present a concern because the reinforcing steel in the concrete (in the hoop and meridional directions) is still in the elastic regime. Thus, the reinforcing bars would be able to carry the overburden loads upon reimpact.

Conclusions of this structural analysis for the best-estimate MEB hydrogen burn are:

- the tank primary liner will not have a tearing failure,
- concrete cracking in the dome does not present a problem for soil reimpaction,
- overall structural integrity of the tank is maintained, and
- high-frequency vibrations from radial rebar do not pose a concern.

3.0. BEST-ESTIMATE MEB (10,480-ft^3) BURN CASE FOR AN MPR VENT FLOW
AREA OF 0%

We must consider the structural adequacy of the tank for a best-estimate gas composition burn case where there is no vent flow through the MPR. The best-estimate MEB burn case with a 0% vent-flow area through the MPR is a 10,480-ft^3 GRE producing a maximum pressure of 3.93 bar (56.9 psia), as shown in Fig. 67. This case was evaluated to determine whether, under best-estimate conditions of gas composition/release rates and no relief flow, an MEB burn would cause structural failure to Tank 101-SY.

The results show a marginal condition to structural acceptability. The complete dome structure resonates at a high frequency throughout the transient, as depicted by the velocity-time histories shown in Figs. 68 and 69. In view of the high-frequency response, the acceleration-time history plots are quite erratic and are not included herein.
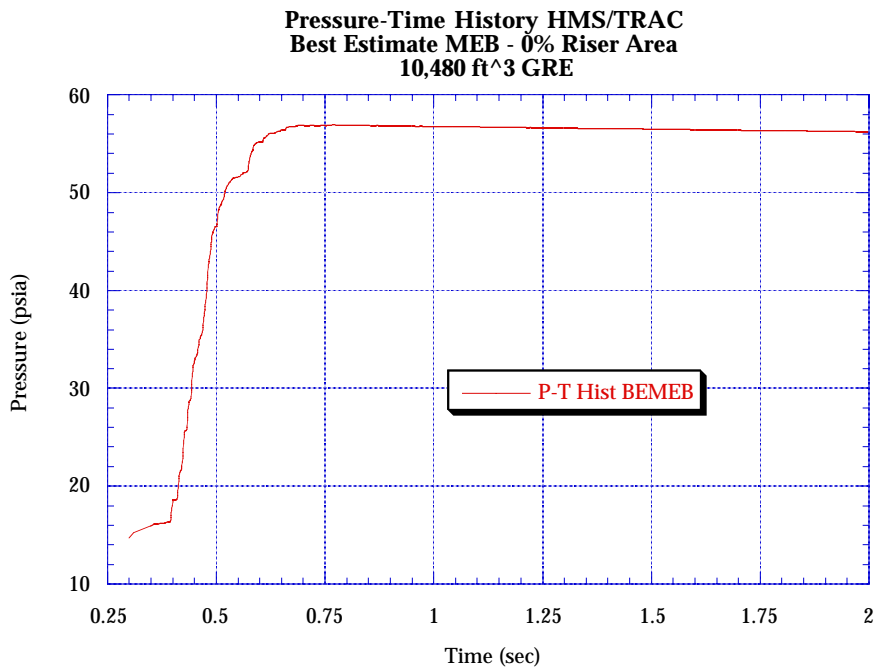
Fig. 67. P-T history for an MEB case with a 0% riser area.

Velocity-Time History Selected Locations
Best Estimate MEB - 0% Riser Area
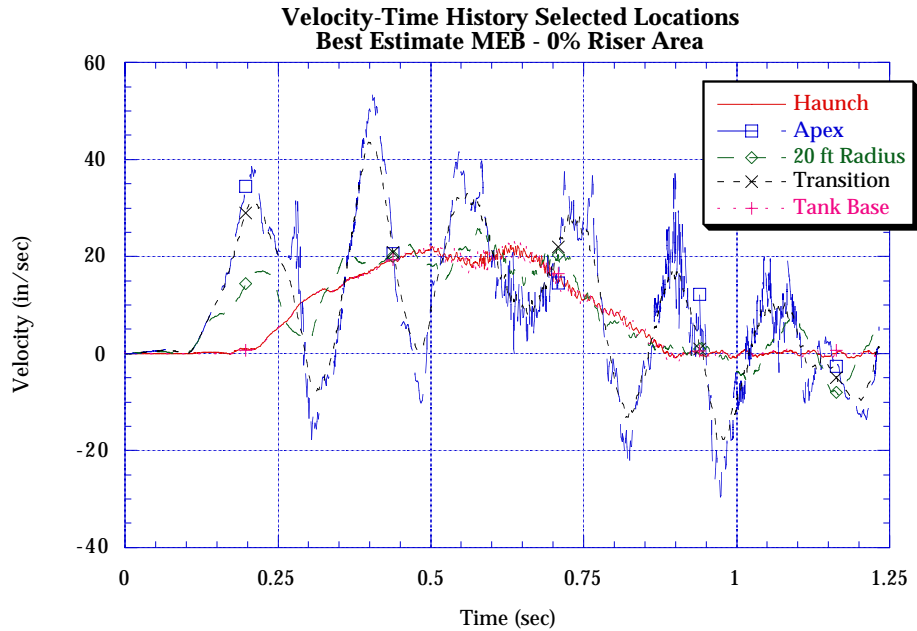
Fig. 68. Velocity-time history for an MEB case with a 0% riser area.

One important parameter shown in Fig. 69 is the maximum velocity of the dome apex, which exhibits 54 in./s. As previously noted, the critical velocity to cause dome failure from reimpaction of the soil overburden and pump pit is 54.5 in./s. Therefore, this resulting dome apex velocity is close to the critical velocity for failure. Additional response parameters are shown in Figs. 70 and 71.

Velocity-Time History Dome Apex
Best Estimate MEB - 0% Riser Area
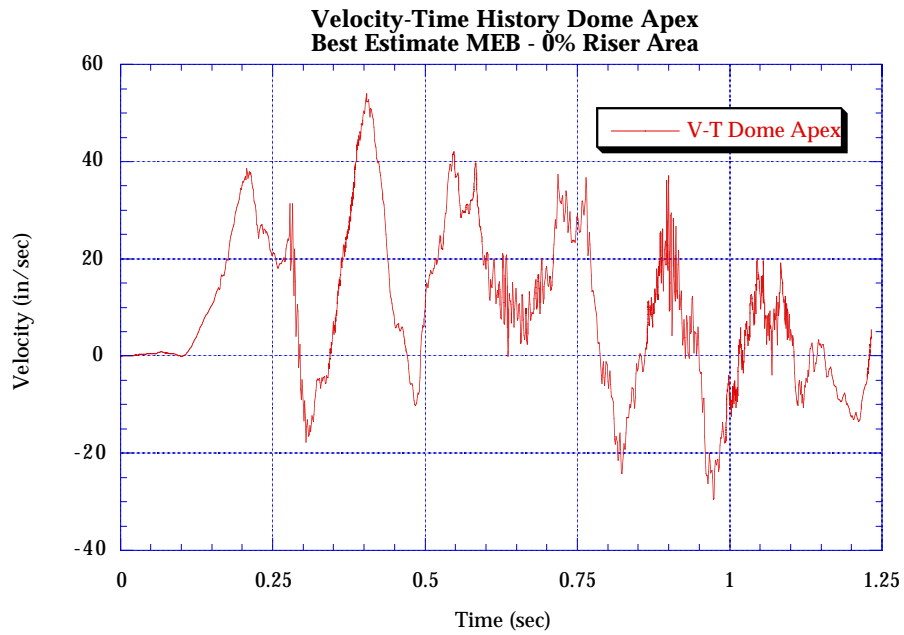
Fig. 69. Velocity-time history at dome apex for an MEB case with a 0% riser area.

Velocity-Time History @ MPR Location
Best Estimate MEB - 0% Riser Area
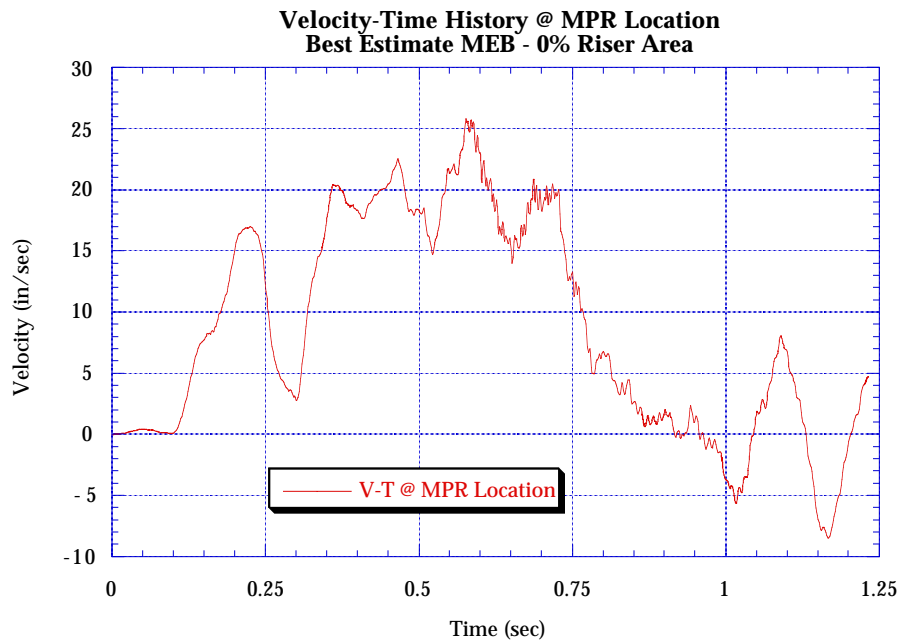
Fig. 70. Velocity-time history for an MPR MEB case with a 0% riser area.

Velocity-Time History Tank Base
Best Estimate MEB - 0% Riser Area
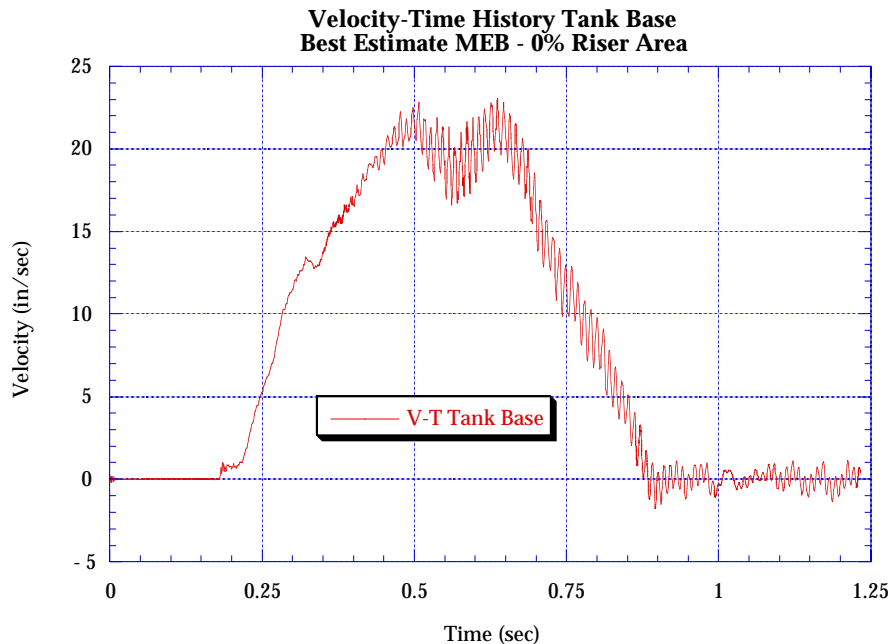
Fig. 71.   Velocity-time history at tank basewall for an MEB case with a 0% riser area.

Results of primary liner plastic strains and dome rebar are found in Table 7.

TABLE 7
TOTAL PLASTIC STRAINS AT SELECTED LOCATIONS

Item	Strain (%)	Limit (%)	Location
Dome Liner	0.4	1.0	Transition
Primary Liner	1.5	6.0	Lower Knuckle
Rebars	0.4	6.0	Dome

Based on the results presented above, there is a slight potential for dome failure with this burn case because the dome apex maximum velocity is in close proximity to the critical velocity for reimpaction of soil and pump pit.

The preceding results have shown that Tank 101-SY can maintain structural integrity for a best-estimate MEB GRE burn with 0% vent-flow area through the MPR, which produces a peak pressure of 3.93 bar (56.9 psia). Structural damage to Tank 101-SY is moderate, with a large portion of the concrete in the dome cracked

and rebar yielding. Primary liner plastic strains are within acceptable limits, and no liner tearing failure is expected.

The analysis performed to quantify the MPR venting capability shows a marked benefit for including the MPR(s). For a given gas volume causing a burn, the peak pressures decrease with increasing relief riser openings. If the MPR doors fail to open, thus providing no relief, the structural adequacy of the tank is maintained. However, this does not imply that there is no need for an MPR. On the contrary, it implies that the benefits of the MPR prevent structural damage under specific burn scenarios.

4.0.   SUMMARY FOR APPENDIX C

Results for the best-estimate gas composition and gas release rate burn scenario show that Tank 101-SY would maintain structural integrity for an MEB gas release of 10,480 ft^3 for vent-flow conditions of both 100 and 0% flow. For the condition of 0% vent-flow area through the MPR, the maximum dome apex velocity is very close to the critical velocity to cause dome failure from soil and pump pit reimpaction. However, we believe that the tank can survive the 0% vent-flow MEB.

5.0.   OVERALL CONCLUSIONS

Structural analyses have been performed for several different burn transients corresponding to conservative estimates and best estimates of gas composition, as well as the volume of gas release and the spark source location. Results show that the response of the tank and dome is very sensitive to the rate of pressurization, as well as the peak pressure attained during the transient.

The top-down burn at the apex of the dome provides the highest initial rate of pressurization (dP/dt). The high rate of pressurization occurs because the flame front takes on a spherical shape, culminating in the maximum amount of surface burn area. That is, the rate of pressurization is proportional to the burn flame-front surface area. Also, the primary liner's thickness transition region is ~6 ft from the apex of the dome. Given the close proximity of the transition region to the apex, the response of the tank (and especially the dome) for a spark source situated at this location would be no more severe than at the apex.

Conversely, a spark source location at the waste surface near the tank wall (which is the burn case of Appendix A) does not have a spherical flame front because of the tank geometry and therefore has a smaller flame surface area. Thus, the rate of pressurization will be much lower.

Given the above discussion, the condition for a spark source at the knuckle region (or haunch) of the tank is quite similar to that of the spark source at the waste

surface near the tank wall. That is, at the knuckle region, a flame front would be moving away from the tank wall toward the waste surface and across the tank. The flame-front geometry in this case is not spherical. The top-down burn is spherical in geometry, but the burn at the waste level and the burn near the knuckle region are somewhat cylindrical in shape. This implies that the flame-front surface area is not as large as the top-down burn; consequently, the rate of pressurization would be somewhat lower. Furthermore, the haunch region structurally is much stiffer than the dome apex, having a thicker concrete cross section and larger amount of steel reinforcing bars in the meridional, hoop, and radial directions. Also, a spark source at the knuckle (or haunch) is not as credible because of limited equipment in that region.

The foregoing analyses show that Tank 101-SY is structurally adequate for the given burn pressure transients provided in Appendices A, B, C and that worst-case pressurization rates have been addressed with the top-down spark source location at the dome apex.

6.0.   FURTHER QUALIFICATIONS

Because structural analyses for the 1.0*MEB top-side burn case were unsuccessful, a complete reanalysis of Tank 101-SY should be developed that minimizes previous conservatisms and includes additional information of the structural response in a degraded material state.

1. Although not probable, an assessment of the benefit in using structural and mass damping will be confirmed for the worst-case burn scenario.

2. An SRS analysis based on the degraded material condition of the tank should be performed to determine the actual degree of amplification.

3. A careful examination of the analytical assumptions, which have been carried throughout the numerous analyses, is recommended in the following areas:

    • The effect of separating the analysis of pressurization from that of the soil/pump pit reimpaction should be considered. The approximate treatment used in Ref. 11 should be scrutinized.

    • A related issue is the critical velocity to cause failure of the dome from reimpaction of the soil and pump pit. The criterion as stated in Ref. 1 limits the peak dome velocity to 54.5 in./s. The accuracy and applicability of the criteria should be verified.

- A more realistic representation of the pressure loading on the tank structure should be used. That is, a spatial-time variation would be more representative than a uniform P-T variation.

- The effect of soil friction should be revisited, first by performing a literature survey of current available data and second by analytical application and comparison of data.

- The overall results of the structural analyses conducted to date must be reviewed by a different independent analysis technique.

REFERENCES

1. L. H. Sullivan et. al., "A Safety Assessment for Proposed Pump Mixing Operations to Mitigate Episodic Gas Releases in Tank 241-SY-101: Hanford Site, Richland, Washington," Los Alamos National Laboratory document LA-UR-92-3196, Rev. 14 (March 1995).

2. E. A. Rodriguez, "Structural Analysis of HLW Tank 101-SY for Top-Side Burn Pressure Transient," Los Alamos National Laboratory calc note TSA6-CN-WT-SA-ST-062 (April 1994).

3. W. D. Birchler and T. A. Butler, "Structural Response of Tank 101-SY to a Postulated Hydrogen Burn," Los Alamos National Laboratory calc note TSA6-CN-WT-SA-ST-067 (September 1994).

4. L. J. Julyk et al., "Structural Integrity Evaluation of Double-Shell-Waste Tank 241-SY-101 under a Postulated Hydrogen Burn," Westinghouse Hanford Company report WHC-SD-WM-TI-465 (April 1990).

5. S. W. Eisenhawer, Los Alamos National Laboratory personal communication, August 1992.

6. R. A. Dameron et al., "Criteria and Guidelines for Predicting Concrete Containment Leakage," ANATECH Research Corporation (April 1989).

7. M. F. Kanninen et al., "Towards an Elastic-Plastic Fracture Mechanics Predictive Capability for Reactor Piping," *Nuclear Engineering and Design* **48**, 117–134 (1978).

8. T. A. Butler and F. W. Smith, "Evaluation of the Crack Plane Equilibrium Model for Predicting Plastic Fracture," in *Fracture, Fatigue, and Advance Mechanics* (American Society of Mechanical Engineers, New York, 1985) PVP Vol. 98-8, pp. 85–91.

9. T. A. Butler, "Failure Criterion at a Crack," Los Alamos National Laboratory calc note N6-CN-WT-SA-ST-028 (August 1992).

10. L. K. Goen, "Dome Analyses," Los Alamos National Laboratory calc note N6-CN-WT-SA-ST-024 (August 1992).

11. T. A. Butler, "Maximum Allowable Separation to Preclude Dome Failure," Los Alamos National Laboratory calc note N6-CN-WT-SA-ST-026 (August 1992).

12. E. A. Rodriguez, "A Simple Model to Predict the Fundamental Frequency of the Reinforced Concrete Dome Structure of High-Level Waste Tank 241-SY101," Los Alamos National Laboratory calc note TSA6-CN-WT-SA-ST-083 (March 1995).